Stem Cell Reports
Article

ISSCR

OPEN ACCESS

Axonal Extensions along Corticospinal Tracts from Transplanted Human Cerebral Organoids

Takahiro Kitahara,[1,2] Hideya Sakaguchi,[1,3,*] Asuka Morizane,[1] Tetsuhiro Kikuchi,[1] Susumu Miyamoto,[2] and Jun Takahashi[1,2,*]

[1]Department of Clinical Application, Center for iPS Cell Research and Application, Kyoto University, Kyoto 606-8507, Japan
[2]Department of Neurosurgery, Kyoto University Graduate School of Medicine, Kyoto 606-8507, Japan
[3]Present address: RIKEN BDR-Otsuka Pharmaceutical Collaboration Center, Kobe 650-0047, Japan
*Correspondence: jbtaka@cira.kyoto-u.ac.jp (J.T.), hideya.sakaguchi@riken.jp (H.S.)
https://doi.org/10.1016/j.stemcr.2020.06.016

SUMMARY

The reconstruction of lost neural circuits by cell replacement is a possible treatment for neurological deficits after cerebral cortex injury. Cerebral organoids can be a novel source for cell transplantation, but because the cellular composition of the organoids changes along the time course of the development, it remains unclear which developmental stage of the organoids is most suitable for reconstructing the corticospinal tract. Here, we transplanted human embryonic stem cell-derived cerebral organoids at 6 or 10 weeks after differentiation (6w- or 10w-organoids) into mouse cerebral cortices. 6w-organoids extended more axons along the corticospinal tract but caused graft overgrowth with a higher percentage of proliferative cells. Axonal extensions from 10w-organoids were smaller in number but were enhanced when the organoids were grafted 1 week after brain injury. Finally, 10w-organoids extended axons in cynomolgus monkey brains. These results contribute to the development of a cell-replacement therapy for brain injury and stroke.

INTRODUCTION

Treatment for neurological sequelae caused by brain injury or stroke is at present limited to medication and rehabilitation, which have some therapeutic effects but cannot provide fundamental cures. On the other hand, the reconstruction of lost neural circuits by a cell-replacement strategy is expected to be a curative therapy for neurological deficits after cerebral cortex injury (Grade and Gotz, 2017; Lindvall and Kokaia, 2011).

The transplantation of embryonic cerebral cortex tissues is an effective approach to reconstructing damaged neural circuits. Previous studies reported that the transplantation of cerebral cortex tissue of mouse embryo into the cerebral cortex of rodents provided axonal projections from the graft to the host brain and spinal cord, synaptic connections between the graft and the host, and functional recovery of the grafted host (Ballout et al., 2016; Gaillard et al., 2007; Peron et al., 2017). Other studies described the transplantation of human pluripotent stem cell (hPSC)-derived neural stem cells, neuronal progenitor cells, or neurons into rodent cerebral cortices to reconstruct neural circuits (Espuny-Camacho et al., 2013, 2018; Palma-Tortosa et al., 2020; Tornero et al., 2013, 2017).

Cerebral organoids are stem cell-derived structures generated *in vitro* and display the 3D architecture and physiology of the cerebrum (Eiraku et al., 2008; Kadoshima et al., 2013; Lancaster et al., 2013; Sakaguchi et al., 2019). They are potential tools for modeling cerebrum-related disorders, such as Zika virus-related microcephaly, and for developing treatments (Cugola et al., 2016; Dang et al., 2016; Garcez et al., 2016; Qian et al., 2016; Watanabe et al., 2017). Since cerebral organoids have a developmental process similar to that of embryonic cerebral cortex, hPSC-derived cerebral organoids can be a cell source for the restoration of lost neural circuits via transplantation. The transplantation of hPSC-derived cerebral organoids into mouse cerebral cortex has been evaluated for the vascularization of the organoids, the rates of graft survival, and the neuronal differentiation after transplantation (Daviaud et al., 2018; Mansour et al., 2018).

Cerebral organoids recapitulate the process of neurogenesis in the development of the cerebral cortex (Heide et al., 2018; Quadrato and Arlotta, 2017; Suzuki and Vanderhaeghen, 2015). *In vivo*, cortical neurogenesis is initiated by rounds of asymmetric divisions of progenitor cells called radial glial cells (RGCs), which form the ventricular zone (VZ) in the apical side of the cerebral cortex. After an asymmetrical division of RGCs, one daughter cell remains as an RGC in the VZ, and the other becomes a neuron or an intermediate progenitor cell. Neurons that migrate out of the VZ form the cortical plate on the basal side of the VZ. Different types of neurons are thought to be generated temporally, and late-born neurons migrate to the basal side of early-born neurons, which results in the unique layer formation of the cerebral cortex with an inside-out pattern (Dwyer et al., 2016; Greig et al., 2013; Kwan et al., 2012; Toma and Hanashima, 2015). The deep layer of the cerebral cortex is formed earlier and contains subcerebral projection neurons (SCPNs), which extend axons to the outside of the cerebral cortex, such as the brainstem and the spinal cord. The upper layer is formed later and composed of callosal projection neurons

(CPNs), which extend axons to other areas of the cerebral cortex (Leyva-Diaz and Lopez-Bendito, 2013; Molyneaux et al., 2007; Toma and Hanashima, 2015). In mouse embryo, SCPNs are generated at approximately embryonic days (E) 12.5–14.5, and CPNs are generated at approximately E13.5–E16.5 (Fame et al., 2011; Hevner et al., 2003; Kwan et al., 2012). Previous studies describing the transplantation of embryonic cerebral cortex generally used E14–E15 mouse cerebral cortex tissues as the grafts (Ballout et al., 2016; Gaillard et al., 2004, 2007; Peron et al., 2017).

Because the cellular compositions of embryonic cerebral cortex and cerebral organoids dramatically change along the time course of the development, differences in the developmental stages of the graft could greatly affect the results of the transplantation. However, the effect of these differences has not been compared in the transplantation of embryonic cerebral cortex and cerebral organoids. Furthermore, in cerebral organoid transplantation, the effect of the transplantation site, the effect of the host brain environment, and the applicability of the transplantation to primates have not been investigated.

In this study, to clarify which developmental stage of cerebral organoids is suitable for transplantation, we transplanted human embryonic stem cell (hESC)-derived cerebral organoids at early stage (the time of SCPN generation) and late stage (the time of CPN generation) into mouse cerebral cortex and compared the graft survival and axonal extension to the host. We also evaluated the effects of the transplantation site and host brain environment as well as the transplantation of cerebral organoids into the motor cortex of nonhuman primate brain.

RESULTS

Characterization of Cerebral Organoids at Different Developmental Stages

For the induction of cerebral organoids, we adopted the serum-free floating culture of embryoid body-like aggregates with a quick reaggregation method (Eiraku et al., 2008; Kadoshima et al., 2013) and our previous protocol (Sakaguchi et al., 2019) (Figure 1A). A total of 9,000 dissociated hESCs were put into each well of low-cell-adhesion-coated 96-well plates, where they formed aggregates efficiently after the initiation of differentiation. The formation of several cricoid neuroepithelium-like structures in the aggregates was observed in bright-field images (Figure 1B). Immunohistochemistry (IHC) analysis of the cerebral organoids at 6 weeks after the initiation of differentiation (6w-organoid) showed the expression of the telencephalic marker FOXG1 (Figure 1C). 6w-organoids contained the VZ, which was composed of RGC-like cells positive for the dorsal telencephalic progenitor marker PAX6, and cells positive for the neuronal marker MAP2 surrounded the VZ (Figure 1C). The proliferation marker KI67 was expressed in many cells in the VZ, validating the proliferative activity of RGC-like cells in the VZ (Figure 1C). Cells positive for the SCPN marker CTIP2 had commenced to form the layer corresponding to the cortical plate while cells positive for the CPN marker SATB2 were not observed (Figure 1C).

In cerebral organoids at 10 weeks after the initiation of differentiation (10w-organoid), the size of neuroepithelium-like structures was larger compared with those of 6w-organoids (Figure 1B). IHC analysis of the 10w-organoids showed that the thickness of the total epithelium was also increased (6w, 142.1 ± 33.3 μm; 10w, 285.1 ± 28.8 μm) (Figure 1D). The increase in thickness was more prominent in the layer of $CTIP2^+$ cells than in the layer of $PAX6^+$ cells, which suggested the robust generation of SCPNs by asymmetric cell division ($PAX6^+$ layer, 89.8 ± 17.0 μm [6w] and 96.9 ± 8.1 μm [10w]; $CTIP2^+$ layer, 29.3 ± 8.5 μm [6w] and 127.7 ± 22.9 μm [10w]) (Figure 1D). The percentages of $PAX6^+$ cells and $KI67^+$ cells in total cells of the organoid were lower in 10w-organoids than in 6w-organoids (PAX6, 44.7% ± 4.8% [6w] and 24.6% ± 7.1% [10w]; KI67, 34.5% ± 5.6% [6w] and 12.5% ± 5.4% [10w]) (Figure 1E). In contrast, the percentage of $CTIP2^+$ cells was higher in 10w-organoids than in 6w-organoids (6w, 25.5% ± 6.3%; 10w, 46.8% ± 9.3%) (Figure 1E). $SATB2^+$ cells, which were absent in 6w-organoids, were evident in 10w-organoids (6.2% ± 5.1%) (Figure 1E). When dividing cells were labeled with 5-ethynyl-2′-deoxyuridine (EdU) in 6w-organoids, the EdU^+ cells contained 5.9% ± 2.2% of $CTIP2^+$ cells but no $SATB2^+$ cells 1 week after the labeling. In contrast, when dividing cells were labeled in 10w-organoids, the EdU^+ cells contained more $SATB2^+$ cells (2.9% ± 1.0%) than $CTIP2^+$ cells (1.8% ± 0.1%) (Figure S1).

These results showed that our culture system could recapitulate the cerebral cortical developmental process, and that 6w-organoids were at a developmental stage before the initiation of CPN generation (early stage) and 10w-organoids were at a developmental stage after the initiation of CPN generation (late stage). We used early- and late-stage organoids as grafts for the transplantations below.

Graft Overgrowth after Transplantation Was Obvious in 6w-Organoids

Next, to evaluate whether the difference in the developmental stage of the organoids and the difference in the site of transplantation affected engraftment, we transplanted 6w- or 10w-organoids into the brain of 7-day-old (P7) mice. The organoids at both stages were cut into pieces with 1 mm diameter, each containing 1.9×10^5 cells on average, and the pieces were implanted into the bilateral frontal and parietal cortices (Figures 2A–2C).

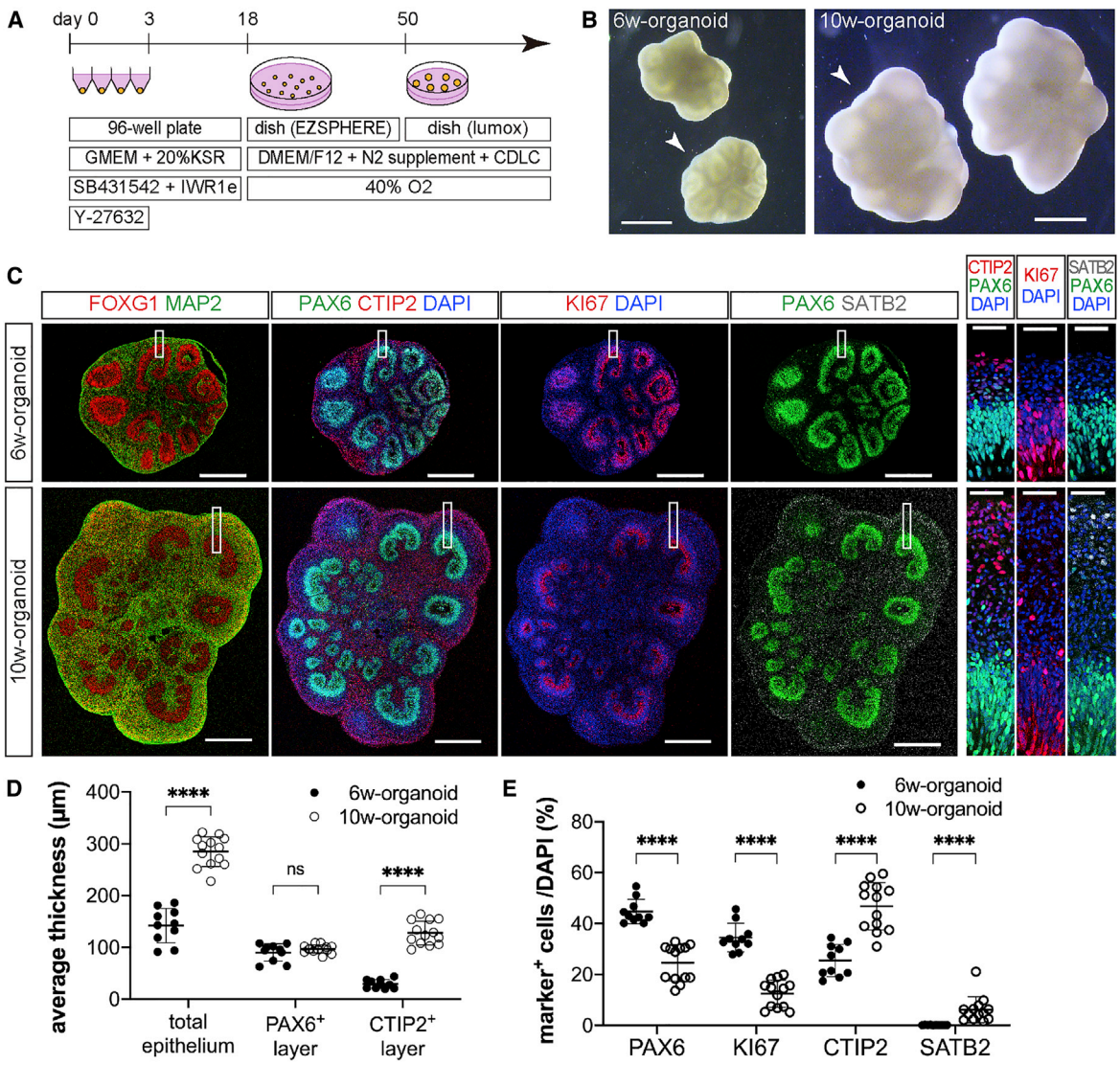

Figure 1. Characterization of Cerebral Organoids at Different Stages Based on Cellular Components

(A) Schematic of the conditions used to induce cerebral organoids from hESCs.

(B) Bright-field images of 6w- and 10w-organoids induced from hESCs. Arrowheads: organoids shown in (C). Scale bars, 1 mm.

(C) Immunohistochemistry for FOXG1, MAP2, PAX6, CTIP2, KI67, and SATB2 in 6w- and 10w-organoids. In 10w-organoids, the layer of $CTIP2^+$ cells was thicker, and $SATB2^+$ cells appeared. Right three columns: higher-magnification images of the corresponding boxed areas. Scale bars, 500 μm (left four columns) and 50 μm (right three columns).

(D) Thickness of the total epithelium, the layer of $PAX6^+$ cells, and the layer of $CTIP2^+$ cells in 6w- and 10w-organoids. Average thickness in each aggregate was used for the analysis. n = 10 for 6w-organoids, and n = 13 for 10w-organoids (n, number of aggregates). ****$p < 0.0001$; ns, not significant, Mann-Whitney test. Results are presented as the mean ± standard deviation.

(E) Percentages of $PAX6^+$ cells, $KI67^+$ cells, $CTIP2^+$ cells, and $SATB2^+$ cells in 6w- and 10w-organoids. The whole area of each aggregate was analyzed. n = 10 for 6w-organoids, and n = 13 for 10w-organoids (n, number of aggregates). ****$p < 0.0001$, Mann-Whitney test. Results are presented as the mean ± standard deviation.

See also Figure S1.

At 12 weeks post-transplantation (wpt), IHC analysis with staining of human neural cell adhesion molecule (hNCAM) revealed the engraftment of 6w- and 10w-organoids in the mouse cerebral cortex (Figure 2D). 6w-organoids enlarged massively to protrude from the transplanted cavities and spread over the surface of the cerebral cortex. On the other hand, 10w-organoids did not cause massive overgrowth of the grafts (Figure 2D). Both 6w- and

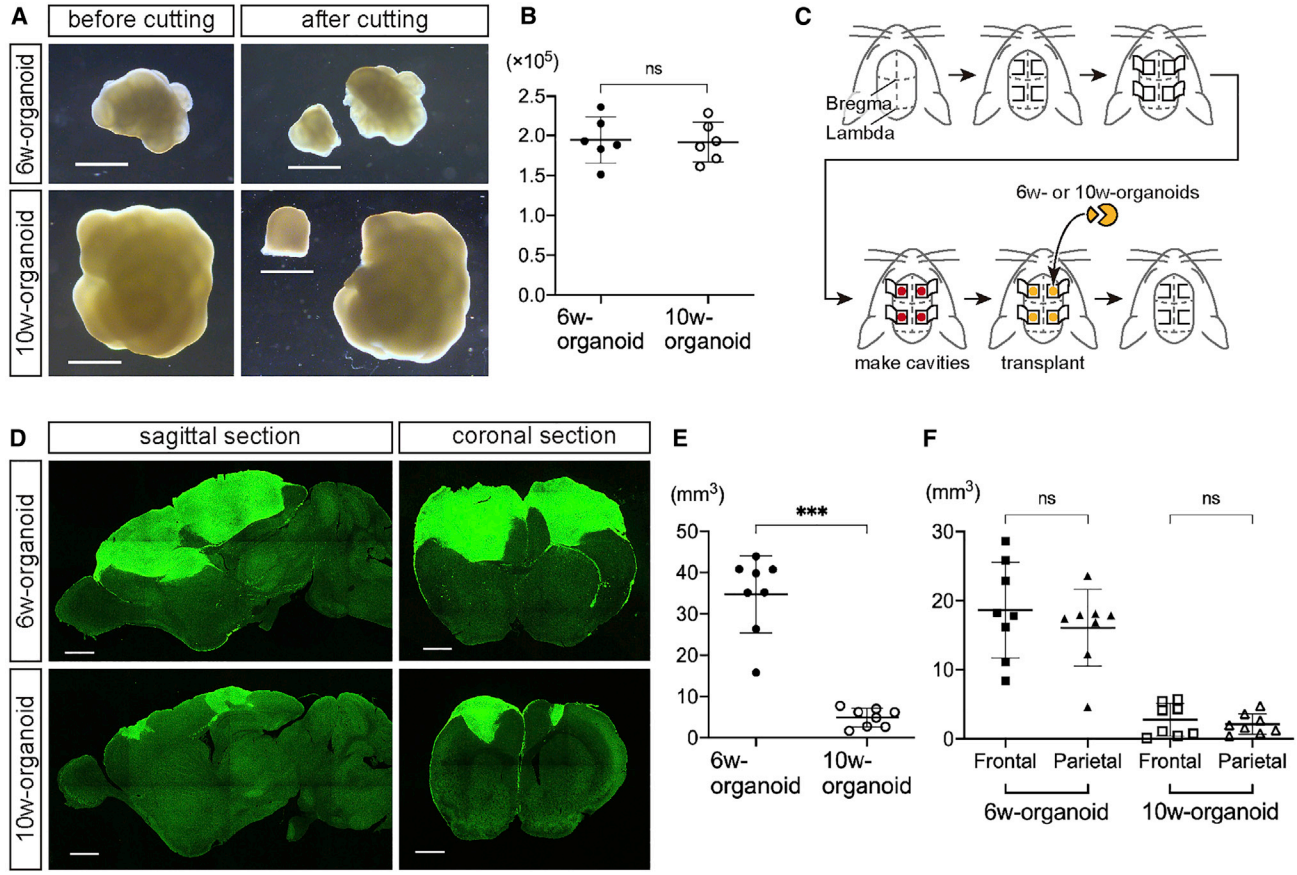

Figure 2. Graft Overgrowth after Transplantation was Obvious in 6w-Organoids

(A) Bright-field images of 6w- and 10w-organoids before and after cutting into pieces. Scale bars, 1 mm.

(B) The number of cells contained in 1-mm pieces of 6w- and 10w-organoids. n = 6 for both organoids (n, number of aggregates). ns, not significant; Mann-Whitney test. Results are presented as the mean ± standard deviation.

(C) Schematic of the procedure for the transplantation of cerebral organoids into the bilateral frontal and parietal cortices of 7-day-old mice (one piece into each cavity).

(D) Immunohistochemistry for hNCAM in sagittal and coronal sections of mouse brains at 12 wpt. Upper left, lateral 1.08 mm; lower left, lateral 1.44 mm; right, Bregma +1.26 mm. Scale bars, 1 mm.

(E) The total volume of all survived grafts in each mouse at 12 wpt. n = 8 for each organoid (n, number of mice). ***$p < 0.001$, Mann-Whitney test. Results are presented as the mean ± standard deviation.

(F) The total volume of all survived grafts in the frontal or parietal cortices of each mouse at 12 wpt. n = 8 for each organoid (n, number of mice). ns, not significant; Wilcoxon test. Results are presented as the mean ± standard deviation.

See also Figure S5.

10w-organoids showed high graft survival rates in both the frontal and parietal cortices (6w, 100%; 10w, 87.5% [frontal] and 93.8% [parietal]). The total graft volume in each mouse at 12 wpt was significantly larger in 6w-organoids than in 10w-organoids (6w, 34.7 ± 9.4 mm^3; 10w, 4.9 ± 2.3 mm^3) (Figure 2E), but with no difference in the graft volume depending on the site of transplantation (Figure 2F). There was no difference in the volume of the host brain irrespective of the culture period of the organoids (6w, 190.5 ± 19.5 mm^3; 10w, 196.8 ± 8.6 mm^3), suggesting that the grafts grew independent of the developmental process of the brain. Both organoids included endothelial cell marker CD31-positive vessel-like structures, suggesting that the cerebral organoids were vascularized from the host environment after the transplantation (Figure 3A). There was no difference in the percentage of the $CD31^+$ area to total graft area (6w, 0.69% ± 0.07%; 10w, 0.72% ± 0.15%) (Figure 3B).

In summary, cerebral organoids at both developmental stages had high rates of graft survival with vascularization, but the risk of graft overgrowth appeared higher in 6w-organoids.

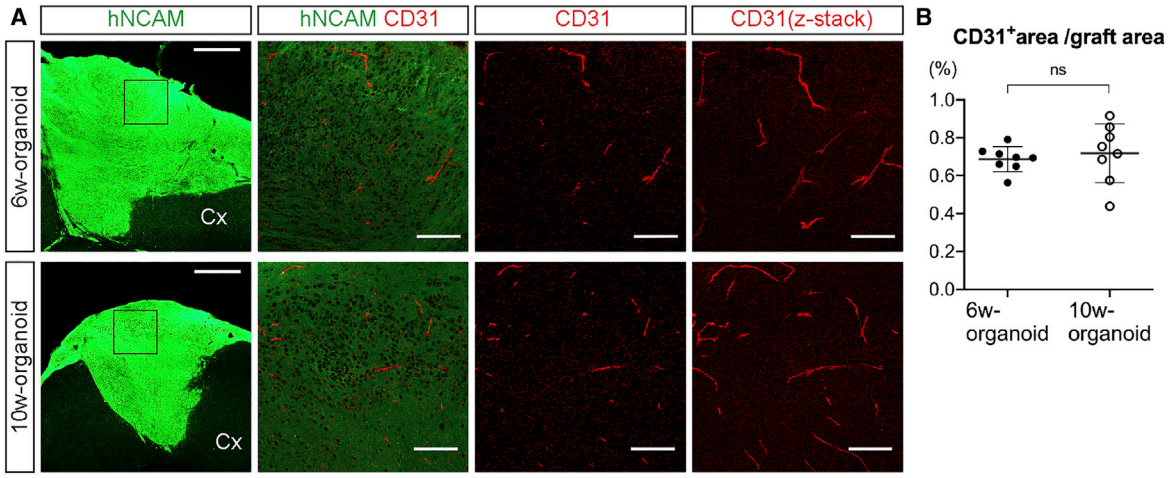

Figure 3. Engrafted Cerebral Organoids Obtained Vascularization from the Host

(A) Immunohistochemistry for hNCAM and CD31 in engrafted 6w- and 10w-organoids. Cx, cerebral cortex. The right three columns show higher-magnification images of the boxed areas. Scale bars, 500 μm (leftmost column) and 100 μm (other columns).

(B) The percentage of the $CD31^+$ area to the $hNCAM^+$ area in engrafted 6w- and 10w-organoids. n = 8 for each organoid (n, number of mice). ns, not significant; Mann-Whitney test. Results are presented as the mean ± standard deviation.

Cerebral Projection Neurons Were Observed in Engrafted Cerebral Organoids, but 6w-Organoids Contained a Higher Percentage of Proliferative Cells

Next, we evaluated whether the overgrowth of 6w-organoids after transplantation was related to their proliferative activity. In 6w-organoids at 12 wpt, the existence of $PAX6^+$ cells was obvious, and some of these cells co-expressed KI67 (Figure 4A). In contrast, in 10w-organoids at 12 wpt, $PAX6^+$ cells were only present sparsely, and few $KI67^+$ cells were observed (Figure 4A). The percentages of $PAX6^+$ cells and $KI67^+$ cells in human nuclei (hNuclei)-positive cells were significantly higher in 6w-organoids than in 10w-organoids (PAX6, 18.5% ± 3.8% [6w] and 9.8% ± 1.8% [10w]; KI67, 5.5% ± 1.0% [6w] and 2.0% ± 0.6% [10w]) (Figures 4B, S2A, and S2B), indicating that 6w-organoids contained a significantly higher percentage of proliferative cells than 10w-organoids not only at the time of transplantation but also at 12 wpt.

To reconstruct host neural circuits by cerebral organoid transplantation, projection neurons are required. Therefore, we next evaluated whether projection neurons existed in the engrafted cerebral organoids. Both 6w- and 10w-organoids contained $CTIP2^+$ cells and $SATB2^+$ cells at 12 wpt (Figure 4C), and both contained more $SATB2^+$ cells than $CTIP2^+$ cells in $hNuclei^+$ cells (Figures 4D and S2C). The percentage of $CTIP2^+$ cells in $hNuclei^+$ cells was significantly higher in 6w-organoids (6w, 15.3% ± 2.9%; 10w, 4.4% ± 1.3%). In contrast, the percentage of $SATB2^+$ cells in $hNuclei^+$ cells was significantly higher in 10w-organoids (6w, 48.8% ± 2.3%; 10w, 63.8% ± 8.0%).

In summary, both 6w- and 10w-organoids that engrafted in the cerebral cortex contained graft-derived projection neurons, including $CTIP2^+$ SCPNs and $SATB2^+$ CPNs, but 6w-organoids contained a higher percentage of proliferative cells, which might explain the graft overgrowth.

6w-Organoids Extended a Larger Number of Axons along the Host Corticospinal Tract

Since cerebral organoids that engrafted in the mouse cerebral cortex contained projection neurons, we investigated how the engrafted cerebral organoids extended axons to the host brain. Both 6w- and 10w-organoids in the frontal cortex extended $hNCAM^+$ fibers to the surrounding cerebral cortex, the corpus callosum (CC), and the striatum (Str) of the host (Figure 5A). In addition, both organoids that engrafted in the parietal cortex extended $hNCAM^+$ fibers to the surrounding cerebral cortex and CC of the host (Figure 5B).

When we evaluated the extension of graft-derived axons along the corticospinal tract (CST) of the host, $hNCAM^+$ fibers from both organoids reached the internal capsule (IC), the cerebral peduncle (CP), and the cervical spinal cord (SC), confirming axonal projections along the host CST (Figure 5C). In Str, $hNCAM^+$ fibers were extended along myelin basic protein-positive fasciculated bundles, in which SCPN axons are known to travel in rodents (Figure S3) (Sano et al., 2017). There was no obvious difference in the direction of axonal extensions between 6w- and 10w-organoids, but 6w-organoids provided more fibers along the host CST than 10w-organoids (Figure 5D). It is possible that the higher number of axons was due to a higher number of surviving cells in the grafts derived from 6w-organoids. Therefore, we normalized the number of axons to the number of $hNuclei^+$ and $CTIP2^+$

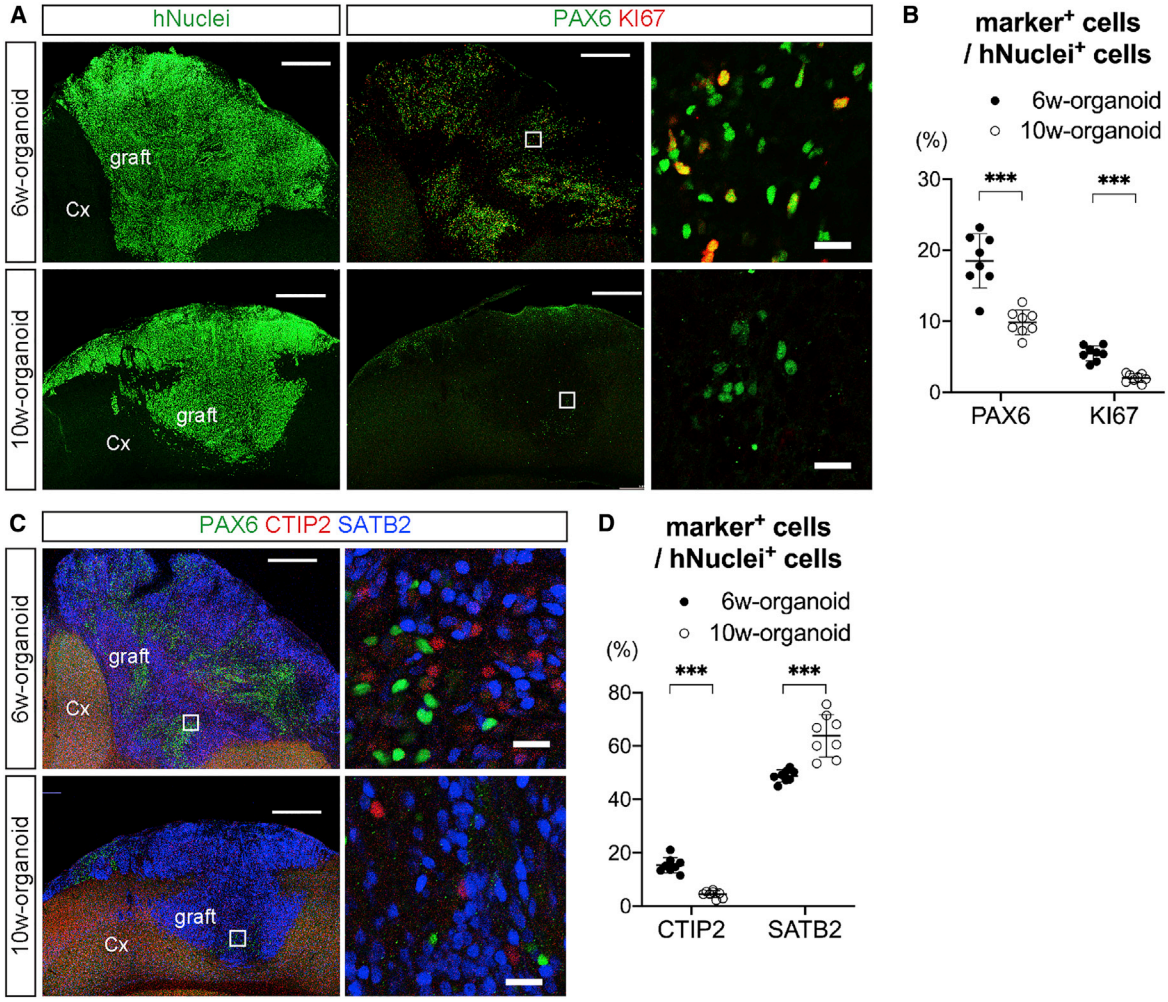

Figure 4. Cerebral Projection Neurons Were Observed in Engrafted Cerebral Organoids, but 6w-Organoids Contained a Higher Percentage of Proliferative Cells

(A) Immunohistochemistry for hNuclei, PAX6, and KI67 in 6w- and 10w-organoids engrafted in the cerebral cortex (Cx). Right column is a magnification of the white squares. Scale bars, 500 μm (left and middle columns) and 20 μm (right column).

(B) Percentages of PAX6$^+$ cells and KI67$^+$ cells in hNuclei$^+$ cells in the engrafted 6w- and 10w-organoids. n = 8 for each organoid (n, number of mice). ***p < 0.001, Mann-Whitney test. Results are presented as the mean ± standard deviation.

(C) Immunohistochemistry for CTIP2, SATB2, and PAX6 in the engrafted 6w- and 10w-organoids. Right column is a magnification of the white squares. Scale bars, 500 μm (left column) and 20 μm (right column).

(D) Percentages of CTIP2$^+$ cells and SATB2$^+$ cells in hNuclei$^+$ cells in the engrafted 6w- and 10w-organoids. n = 8 for each organoid (n, number of mice). ***p < 0.001, Mann-Whitney test. Results are presented as the mean ± standard deviation.

See also Figures S2 and S5.

cells in the grafts. Although the number of axons per hNuclei$^+$ cell was higher in 6w-organoids (Figure S4A), there was no difference in the number of axons per hNuclei$^+$CTIP2$^+$ cell in the Str, CP, and SC (Figure S4B).

These data suggested that both 6w- and 10w-organiods had the ability to provide axonal extensions along the host CST but the number of axons was higher in 6w-organoids, and that CTIP2$^+$ cells in the graft contributed to the axonal extension along the CST.

6w-Organoids Extended More Axons but Caused Overgrowth in Injured Adult Brain

Above, we observed that cerebral organoids extended axons along the CST in the intact brains of P7 mice, but these effects were not confirmed in adult or injured brains. Therefore, we next transplanted 6w- and 10w-organoids into the frontal cortex of 6-week-old mice 1 week after lesioning (Figure S5A). A cavity was made in the right frontal cortex, including the

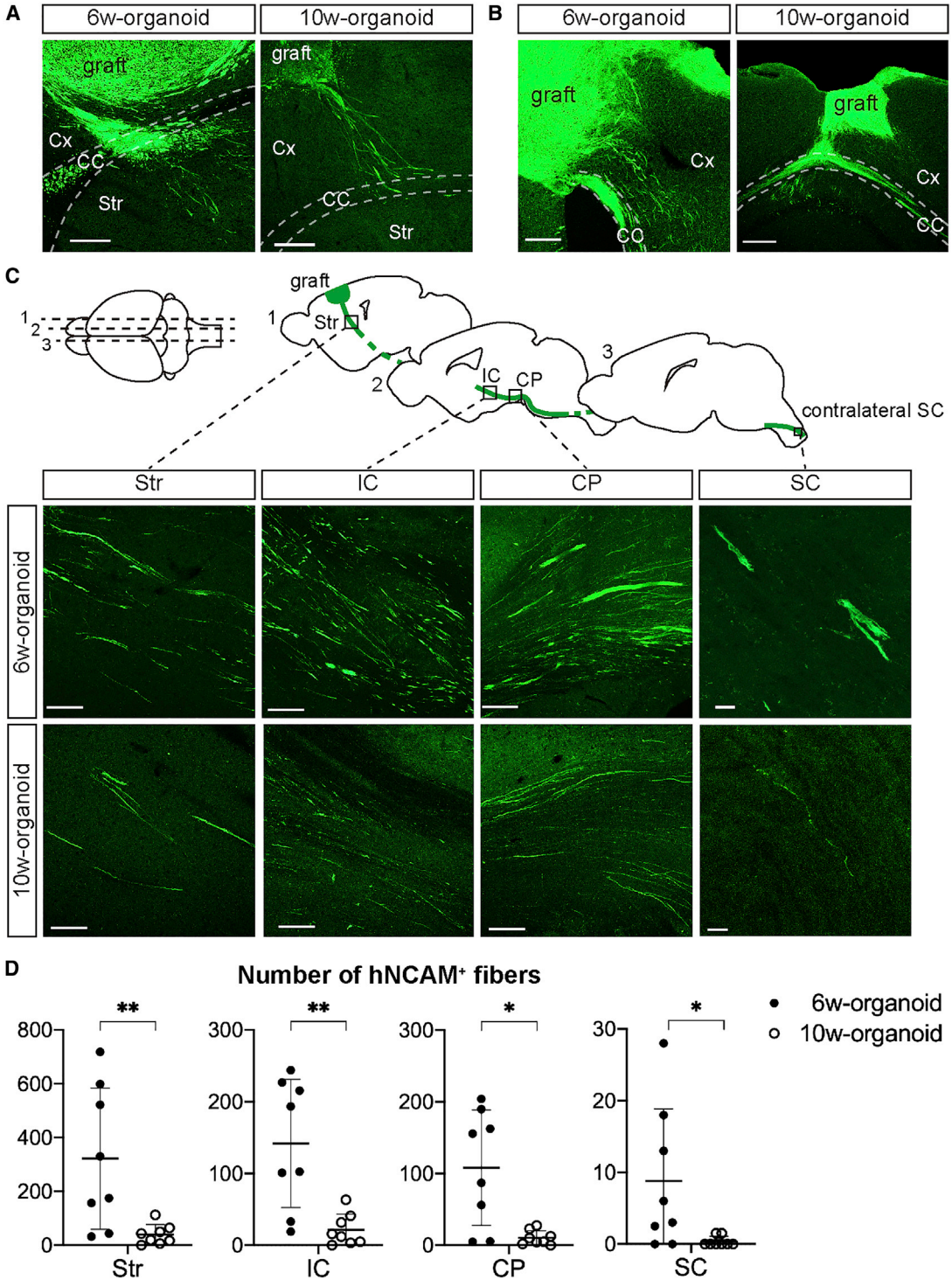

Figure 5. 6w-Organoids Extended More Axons along the Host CST

(A) Immunohistochemistry for human hNCAM after the transplantation of 6w- and 10w-organoids into the frontal cortex (sagittal section) shows graft-derived axonal extensions to the cerebral cortex (Cx), corpus callosum (CC), and striatum (Str). Scale bars, 200 μm.

(B) Immunohistochemistry for hNCAM after the transplantation of 6w- and 10w-organoids into the parietal cortex (coronal section) shows graft-derived axonal extensions to the Cx and CC. Scale bars, 200 μm.

(legend continued on next page)

motor area, and a 1-mm piece of organoids was implanted 1 week later.

The graft volume at 12 wpt was significantly larger in 6w-organoids than in 10w-organoids (6w, 27.0 ± 17.7 mm^3; 10w, 6.7 ± 5.2 mm^3) (Figures S5B and S5C). So too were the percentages of $PAX6^+$ cells and $KI67^+$ cells in $hNuclei^+$ cells (PAX6, 13.6% ± 5.1% [6w] and 7.0% ± 3.4% [10w]; KI67, 4.7% ± 1.1% [6w] and 2.6% ± 1.1% [10w]) (Figures S5D, S5E, and S6A). The percentage of $CTIP2^+$ cells in $hNuclei^+$ cells was significantly higher in 6w-organoids, while that of $SATB2^+$ cells was higher in 10w-organoids (CTIP2, 21.2% ± 8.5% [6w] and 8.3% ± 2.9% [10w]; SATB2, 48.7% ± 9.5% [6w] and 66.6% ± 7.0% [10w]) (Figures S5F, S5G, and S6A). In addition, we observed extensions of $hNCAM^+$ fibers along the host CST in both groups (Figure S5H), but 6w-organoids provided a significantly larger number of axons to the host IC and CP (Figure S5I).

In summary, as in the case of transplantation into P7 mice, 6w-organoids extended a higher number of axons along the host CST but caused graft overgrowth with more proliferative cells in the injured brain of 6-week-old mice.

Axonal Extensions from 10w-Organoids Were Enhanced by Delayed Transplantation after Lesioning

In the transplantation of embryonic cerebral cortex, transplantation 1 week after lesioning in the host cerebral cortex promotes axonal extensions from the graft to the host brain rather than transplantation immediately after lesioning (Peron et al., 2017). We therefore considered that if the cerebral organoids had properties similar to embryonic cerebral cortex, then a 1-week delay could enhance axonal extensions even using 10w-organoids, which provided less axonal growth compared with 6w-organoids. To test this hypothesis, we prepared two groups of transplantation of 10w-organoids into 6-week-old mice: transplantation immediately after lesioning (no-delay group) and 1 week after lesioning (1w-delay group) (Figure 6A), and compared the results of the transplantation between the two groups.

The graft survival rate at 12 wpt was higher in the 1w-delay group than the no-delay group (no-delay, 66.7%; 1w-delay, 100%). Furthermore, the graft volume was significantly larger in the 1w-delay group than in the no-delay group (no-delay, 1.1 ± 0.6 mm^3; 1w-delay, 6.4 ± 1.8 mm^3) (Figures 6B and 6C). However, there was no significant difference in the volume of the host brain (no-delay, 219.2 ± 15.5 mm^3; 1w-delay, 210.9 ± 10.5 mm^3), in the percentage of the $CD31^+$ area to total graft area (no-delay, 0.62% ± 0.20%; 1w-delay, 0.76% ± 0.13%) (Figures 6D and 6E), in the percentages of $PAX6^+$ cells and $KI67^+$ cells in $hNuclei^+$ cells (PAX6, 9.7% ± 3.3% [no-delay] and 10.5% ± 3.5% [1w-delay]; KI67, 2.7% ± 1.6% [no-delay] and 1.9% ± 0.9% [1w-delay]) (Figures 6F, 6G, and S6B), or in the percentages of $CTIP2^+$ cells and $SATB2^+$ cells in $hNuclei^+$ cells (CTIP2, 11.3% ± 5.1% [no-delay] and 10.4% ± 4.5% [1w-delay]; SATB2, 70.8% ± 4.1% [no-delay] and 60.9% ± 6.1% [1w-delay]) (Figures 6H, 6I, and S6B). In both groups, the grafts extended axons along the host CST (Figure 6J), but there was a significantly larger number of $hNCAM^+$ fibers in the 1w-delay group than in the no-delay group (Figure 6K).

In summary, as in the case of transplanting embryonic cerebral cortex, a 1-week delay between lesioning and transplantation enhanced axonal extensions from the 10w-organoids to the host brain, suggesting that neural circuit reconstruction after cerebral organoid transplantation could be promoted by modulating the environment of the host brain.

Cerebral Organoids Extended Axons in the Brains of Nonhuman Primates

Finally, we investigated whether the transplantation of cerebral organoids could be applied to primates. From an ethical point of view, we transplanted hESC-derived 10w-organoids, which had a lower risk of overgrowth that causes compression of the host brain than 6w-organoids, into the cerebral cortex of cynomolgus monkeys. In order not to affect the higher brain functions of the monkeys, we transplanted cerebral organoids only into the bilateral precentral gyrus, namely the primary motor cortex (Figure 7A).

10w-Organoids survived in the cerebral cortex bilaterally in two out of four monkeys at 12 wpt. In the other two monkeys, no graft survival was observed. Using magnetic resonance imaging (MRI), we identified engrafted tissues as regions with high intensity on T2-weighted images and with low intensity on T1-weighted images. There was

(C) Schematic showing sagittal sections of mouse brains, including the (1) Str, (2) internal capsule (IC) and cerebral peduncle (CP), and (3) contralateral spinal cord (SC), and IHC for hNCAM showing graft-derived axonal extensions along the host CST after the transplantation of 6w- and 10w-organoids. Scale bars, 100 μm (left three columns) and 20 μm (rightmost column).

(D) Number of $hNCAM^+$ axons in the Str, IC, CP, and SC of the host after the transplantation of 6w- and 10w-organoids. 6w-organoids provided significantly more axons along the host CST. Average numbers in both hemispheres in each mouse were used for the analyses. n = 8 for each organoid (n, number of mice). *p < 0.05, **p < 0.01, Mann-Whitney test. Results are presented as the mean ± standard deviation.

See also Figures S3–S5.

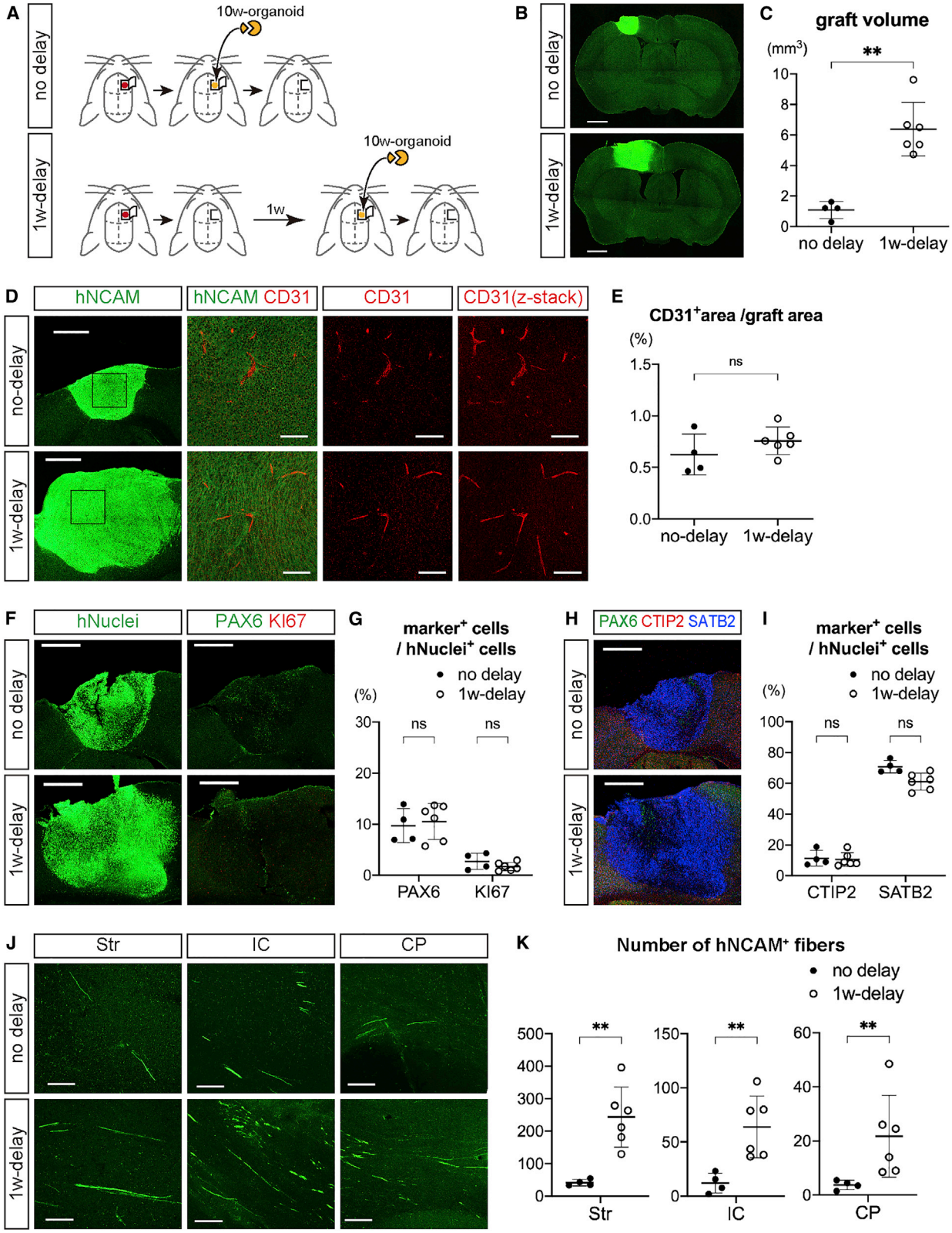

(legend on next page)

no obvious overgrowth of cerebral organoids in any monkey (Figure 7B).

Using IHC analysis, we detected the engraftment of hESC-derived cerebral organoids using the human-specific cytoplasm marker STEM121 (Figures 7B and 7C). Engrafted tissues entirely expressed the neuronal marker TUJ1 (Figure 7C). As was the case of transplantation into mouse cerebral cortex, the engrafted tissues contained more $SATB2^+$ cells than $PAX6^+$ cells, $KI67^+$ cells, and $CTIP2^+$ cells in monkey primary cortex (PAX6, 9.4%; KI67, 2.7%; CTIP2, 6.1%; SATB2, 60.6%) (Figures 7C and 7D). We observed $CD31^+$ vessel-like structures in the graft, suggesting that the cerebral organoids obtained vascularization in the monkey brains (Figures 7E and 7F). IHC analysis with a mouse-specific CD31 antibody and a human/monkey-specific CD31 antibody suggested that the blood vessels in the grafts were derived from the host brain (Figure S7). Engrafted 10w-organoids extended $STEM121^+$ fibers to the brains of the host monkeys. The $STEM121^+$ fibers reached the neighboring cerebral cortical area as well as the subcortical tissue. There were also extensions of $STEM121^+$ fibers in the subcortical tissue both toward the CC and Str (Figure 7G), but there were no fiber extensions in more distal parts, such as the IC or CP.

Taken together, hESC-derived cerebral organoids survived in the cerebral cortex of monkeys and provided axonal extensions along the callosal projection and the subcerebral projection, which suggested that cerebral organoid transplantation could be a useful approach for reconstructing neural circuits after cerebral cortex injury in primates.

DISCUSSION

In this study, we compared the graft volume and axonal extensions along the host CST after transplanting hESC-derived cerebral organoids at two developmental stages. One was the early stage (6w) before the initiation of CPN generation (SCPN-generating stage), and the other was the late stage (10w) after the initiation of CPN generation (CPN-generating stage). We found that the 6w-orgnoids extended a larger number of axons along the host CST, but that they also showed graft overgrowth. In addition, axonal extensions were enhanced in the brain 1 week after brain injury compared with just after the injury. Finally, cerebral organoids survived and extended axons after transplantation into monkey brain.

There are two reports regarding the transplantation of human cerebral organoids into animal brains, but axonal extensions from the organoids along the host CST have never been described. One report showed the vascularization of the organoids with integration to the host brain after transplantation in the mouse retrosplenial cortex (Mansour et al., 2018). The other compared 3D cerebral organoids and 2D culture-derived cells in terms of graft survival and neuronal differentiation in the mouse frontoparietal cortex (Daviaud et al., 2018). In this study, we demonstrated that human cerebral organoids grafted in the mouse frontal cortex extended axons along the CST, suggesting their potential for reconstruction of the host motor pathway.

Figure 6. Axonal Extensions from 10w-Organoids were Enhanced by Delayed Transplantation

(A) Schematic of the procedure for the transplantation of 10w-organoids into the frontal cortex of 6-week-old mice with or without 1-week (1w) delay after lesioning. n = 6 for both groups (n, number of mice).

(B) Immunohistochemistry for hNCAM in coronal sections of mouse brains at 12 wpt with or without 1w delay. Bregma +0.18 mm. Scale bars, 1 mm.

(C) The graft volume at 12 wpt. All mice with graft survival were analyzed (n = 4 for no-delay group, and n = 6 for 1w-delay group). $^{**}p < 0.01$, Mann-Whitney test. Results are presented as the mean ± standard deviation.

(D) Immunohistochemistry for hNCAM and CD31 in engrafted tissues. The right three columns show higher-magnification images of the boxed areas. Scale bars, 500 μm (leftmost column) and 100 μm (other columns).

(E) Percentage of the $CD31^+$ area to the $hNCAM^+$ area in the engrafted tissues. n = 4 for no-delay group, and n = 6 for 1w-delay group (n, number of mice). ns, not significant; Mann-Whitney test. Results are presented as the mean ± standard deviation.

(F) Immunohistochemistry for hNuclei, PAX6, and KI67 in the engrafted tissues at 12 wpt with or without 1w delay. Scale bars, 500 μm.

(G) Percentages of $PAX6^+$ cells and $KI67^+$ cells in $hNuclei^+$ cells in the engrafted tissues at 12 wpt with or without 1w delay. n = 4 for no-delay group, and n = 6 for 1w-delay group (n, number of mice). ns, not significant; Mann-Whitney test. Results are presented as the mean ± standard deviation.

(H) Immunohistochemistry for CTIP2, SATB2, and PAX6 in the engrafted tissues at 12 wpt with or without 1w delay. Scale bars, 500 μm.

(I) Percentages of $CTIP2^+$ cells and $SATB2^+$ cells in $hNuclei^+$ cells at 12 wpt with or without 1w delay. n = 4 for no-delay group, and n = 6 for 1w-delay group (n, number of mice). ns, not significant; Mann-Whitney test. Results are presented as the mean ± standard deviation.

(J) Immunohistochemistry for hNCAM in sagittal sections of mouse brain shows graft-derived axonal extensions in the striatum (Str), internal capsule (IC), and cerebral peduncle (CP) of the host at 12 wpt with or without 1w delay. Scale bars, 100 μm.

(K) Number of $hNCAM^+$ fibers in the Str, IC, and CP of the host at 12 wpt with or without 1w delay. n = 4 for no-delay group, and n = 6 for 1w-delay group (n, number of mice). $^{**}p < 0.01$, Mann-Whitney test. Results are presented as the mean ± standard deviation.

See also Figure S6.

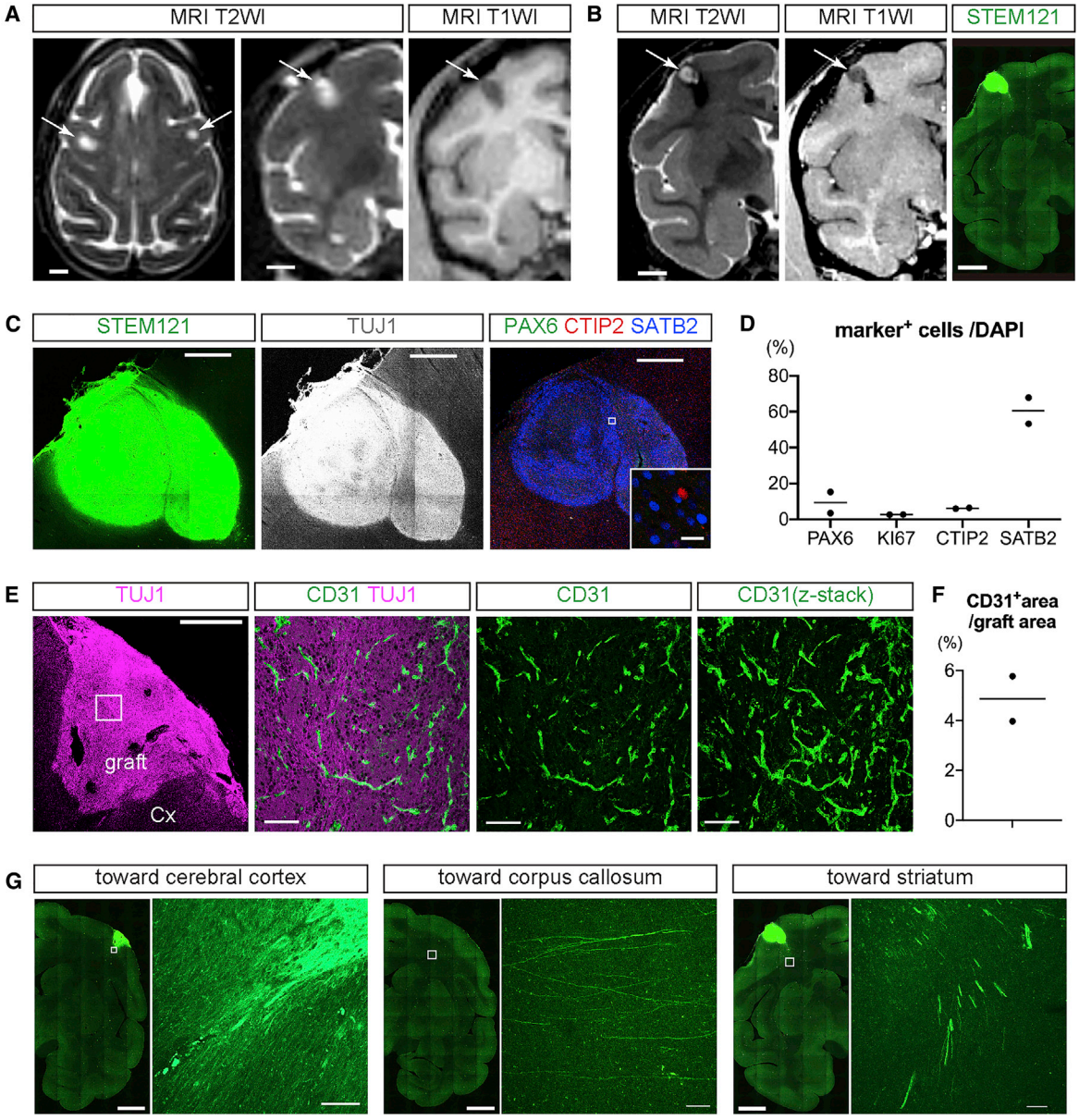

Figure 7. Transplantation of 10w-Organoids into Monkey Cerebral Cortex

(A) Axial (left) and coronal (middle) T2-weighted images (T2WI) and coronal T1-weighted image (T1WI) immediately after the transplantation. Arrows mark the site of the transplantation. Scale bars, 5 mm.

(B) Coronal T2WI and T1WI at 12 wpt, and immunohistochemistry for STEM121 in coronal sections of monkey brain. Scale bars, 5 mm.

(C) Immunohistochemistry for STEM121, TUJ1, PAX6, CTIP2, and SATB2 in the engrafted tissue in monkey cerebral cortex. Scale bars, 1 mm (except inset) and 20 μm (inset).

(D) Percentages of $PAX6^+$ cells, $KI67^+$ cells, $CTIP2^+$ cells, and $SATB2^+$ cells in intragraft cells at 12 wpt. n = 2 (n, number of monkeys).

(E) Immunohistochemistry for TUJ1 and CD31 in the engrafted tissue and the host cerebral cortex. The right three columns show higher-magnification images of the boxed areas. Scale bars, 1 mm (leftmost column) and 100 μm (other columns).

(F) The percentage of the $CD31^+$ area to total graft area. n = 2 (n, number of monkeys).

(G) Immunohistochemistry for STEM121 shows graft-derived axonal extensions to the cerebral cortex and in the subcortical tissues toward the corpus callosum and striatum. Scale bars, 5 mm (low magnification images) and 100 μm (high magnification images).

See also Figure S7.

In the cerebral cortex, SCPNs, which constitute the CST, express CTIP2 (Arlotta et al., 2005) but not SATB2 (Alcamo et al., 2008; Britanova et al., 2008; Fame et al., 2011). It is reported that in the transplantation of dissociated cerebral cortices from mouse embryos, graft-derived cells that extended axons along the host CST are also CTIP2^{+}/SATB2^{-} (Wuttke et al., 2018). In our study, 6w-organoids, which contained more CTIP2^{+} cells than did 10w-organoids at 12 wpt, extended more axons along the host CST, but there was no significant difference in the number of axons per graft-derived CTIP2^{+} cell in the Str, CP, or SC. These results suggest that CTIP2^{+} cells in the graft play a pivotal role in reconstruction of the CST. It remains unclear, however, what stage of cells in the organoids contributed to the axonal extensions. We suspect two candidates: one is projection neurons that already exist in the graft at the time of transplantation, and the other is immature cells that become projection neurons after the transplantation. In a previous report, graft-derived axons along the host CST were provided by cells that were already post-mitotic at the time of transplantation (Wuttke et al., 2018). In this study, compared with 10w-organoids, 6w-organoids contained less CTIP2^{+} cells at the time of transplantation, but provided more CTIP2^{+} cells with a larger number of axons after transplantation. This result might suggest that more post-transplant-generated CTIP2^{+} cells became projection neurons, which extended axons along the CST, compared with already-existing CTIP2^{+} cells.

In cell transplantation toward clinical application, graft overgrowth must be avoided because it causes compression or destruction of the host brain. However, the risk of graft overgrowth has not been investigated in cell transplantations aimed at cerebral cortex repair. We found that 10w-organoids, which are in the CPN-generating stage, have a lower risk of graft overgrowth. In previous studies describing the transplantation of embryonic cerebral cortex, E14–E15 mice, which corresponds to the CPN-generating stage, were used as the grafts (Ballout et al., 2016, 2019; Gaillard et al., 2004, 2007; Peron et al., 2017), which would explain why graft overgrowth did not become a problem in those studies.

The observed enhancement of the graft survival and axonal extensions of 10w-organoids by delaying the transplantation 1 week after the cortical resection suggests that adjusting the host brain environment is a possible approach to promoting axonal extensions from cerebral organoids. Our result is in agreement with a previous study that examined embryonic cerebral cortex (Peron et al., 2017). However, the mechanism through which the host brain 1 week after the resection supports cell survival and axonal extension is unknown. Previous studies suggest that the secretion of pro-angiogenic factors by cells surrounding the lesion (Skold et al., 2005) or the modulation of inflammatory responses (Ballout et al., 2019; Liauw et al., 2008) are candidates. It is reported that transplantation with 1-week delay provided a transient increase in graft vascularization 4 days after the transplantation (Peron et al., 2017). In our study, a 1-week delay did not cause an obvious difference in the graft vascularization at 12 wpt, but a transient increase in the graft vascularization might have contributed to the enhancement of axonal extensions.

There are substantial differences in the nervous systems between rodents and primates in terms of size and neuroanatomical characteristics (Courtine et al., 2007). For example, in rodents, CST fibers descending in the spinal cord travel mostly in the dorsal columns and have no direct connections to motor neurons. In contrast, in primates, CST fibers in the spinal cord travel mostly in the lateral columns and have both direct and indirect connections to motor neurons (Courtine et al., 2007; Lemon, 2008). Such differences can limit the translation of the results obtained from rodents into treatment for human patients (Courtine et al., 2007). Therefore, when considering clinical application, primate transplantation models are necessary. One report more than 30 years ago transplanted allogenic embryonic cerebral cortex tissues into the brain of rhesus monkeys, but no graft survival was observed in the cerebral cortex (Gopinath et al., 1989). The current study clearly showed that the transplantation of hPSC-derived cells into the primate cerebral cortex resulted in graft survival and axonal extensions. The axons, however, were observed only in the subcortical area, probably because a 12-week observation is too short when considering the size of monkey brains. Observation over longer periods is needed to confirm axonal extensions for longer distances.

Ethical issues need to be considered in experiments in which human cells are transplanted into the cerebral cortex of animals (Chen et al., 2019). In this study, to avoid the risk of manipulating the higher brain functions of monkeys by transplantation, we limited the transplantation site to the motor cortex. In addition, to avoid the risk of graft overgrowth compressing the monkey brain, only 10w-organoids were transplanted. Furthering this type of research will include ethical concerns, such as whether the animals can be humanized by creating brain chimeras and whether the cerebral organoids *in vitro* can have consciousness (Sawai et al., 2019).

Optimization of both the donor cells and host brain environment is critical for successful transplantations. We have shown that early-stage organoids extend more axons but cause graft overgrowth. Elimination of the proliferating cells by sorting may solve this problem (Samata et al., 2020). In parallel, the clarification and administration of supportive factors may enhance graft survival and axonal extensions. Stepwise solution of these issues will open

the way to the realization of a cell-based therapy for brain injury and stroke.

EXPERIMENTAL PROCEDURES

Animals

All animal experiments described in this study were approved by the Institutional Animal Care and Use Committee of the Animal Research Facility at Kyoto University. All animals were cared for and handled in accordance with the Regulation on Animal Experimentation at Kyoto University.

SCID mice (C.B-17/IcrHsd-Prkdcscid, Shimizu Laboratory Supplies) 7 days (male and female, n = 16) and 6 weeks (male, n = 22) old, and purpose-bred male cynomolgus monkeys (*Macaca fascicularis*, Shin Nippon Biomedical Laboratories, n = 4) 3 years old, were used as the transplant recipients. All mice and monkeys were kept on a 12-h light/dark cycle with *ad libitum* access to food and water.

Surgical Procedure for Mice

All surgical procedures for mice were performed under anesthesia with isoflurane inhalation. In 7-day-old mice, cerebral organoids were transplanted into the bilateral frontal and parietal cortices immediately after making cavities in the cerebral cortices. Half of the mice (n = 8) received 6w-organoids and the other half (n = 8) received 10w-organoids. A skin incision was performed, and 2 × 2 mm craniotomy windows were opened with bone flaps hinged on the lateral base. A cavity of 1 mm diameter and 1 mm depth was made by aspirating the cortical tissue in each craniotomy window. Cerebral organoids were cut into 1-mm-diameter pieces using micro-scissors (Bio Research Center, no. 16324319), and one piece was implanted into each cavity. The craniotomy window was closed by returning the bone flap, and the skin was sutured with 7-0 ETHILON (Ethicon). In 6-week-old mice, 1-mm pieces were transplanted into the right frontal cortex 1 week after (n = 16) or immediately after (n = 6) making the cavity.

Surgical Procedure for Monkeys

All surgical procedures for monkeys were performed under anesthesia with an intramuscular injection of ketamine (10 mg/kg) and xylazine (1 mg/kg). Bilateral precentral gyri were identified by preoperative MRI, and the coordinates of the targets were obtained. A midline skin incision was performed, and 10-mm burr holes were made above the bilateral precentral gyri based on the coordinates obtained from the preoperative MRI. The dura mater was incised, and a 2-mm cavity was made in the precentral cortex. 10w-Organoids were cut into 1-mm pieces, and 3, 5, or 11 pieces were implanted into each cavity. The dura mater and epicranial aponeurosis were sutured with 4-0 NUROLON (Ethicon), and the skin was sutured with 4-0 NESCOSUTURE (alfresa).

An antibiotic (cefazolin sodium; Astellas Pharma) was administered for 3 days from the day of the operation (70 mg/body, intramuscularly). An immunosuppressant (Tacrolimus hydrate; Towa Pharmaceutical, prepared at 5 mg/mL in ethanol and polyoxyethylene hydrogenated castor oil 60) was administered from 1 day before transplantation until the day of euthanization (0.05–0.075 mg/kg, intramuscularly). The blood trough concentration of Tacrolimus was monitored and maintained at 10–25 ng/mL, with blood sampling once every week until the blood concentration reached within the target range followed by blood sampling at 4, 8, and 12 wpt.

Data Acquisition

Images were obtained using a confocal laser microscope (LSM710 and LSM800, Zeiss), except images for quantitative analyses and images of wide fields (Figures 2B, 5B, 6B, and 7B, left two images of 7C, and lower-magnification images of 7G), which were obtained using a confocal quantitative image cytometer (CQ1; Yokogawa).

Statistical Analysis

Statistical analyses were performed with PRISM software (GraphPad, version 8). Statistical significances in two-group comparisons were tested with the Mann-Whitney test (unpaired, nonparametric), except the comparison of graft volume in the mouse frontal and parietal cortices (Figure 2D), which was tested with the Wilcoxon test (paired, nonparametric). The results are expressed as the mean ± standard deviation.

SUPPLEMENTAL INFORMATION

Supplemental Information can be found online at https://doi.org/10.1016/j.stemcr.2020.06.016.

AUTHOR CONTRIBUTIONS

T.Kitahara, H.S., and J.T. designed the project. T.Kitahara and H.S. performed the research. A.M. and T.Kikuchi assisted with the experiments using monkeys. T.Kitahara and H.S. analyzed the data. T.Kitahara and H.S. wrote the original draft. J.T. reviewed and edited the manuscript. S.M. and J.T. supervised the research. H.S. and J.T. obtained grants for the research. All authors approved the final manuscript as submitted.

ACKNOWLEDGMENTS

The authors thank Takayoshi Matsubara (PerkinElmer Japan Co., Ltd. Imformatics) for technical support in the data acquisition using CQ1 and in the data analysis using CellPathfinder; to Kei Kubota for technical support in experiments using monkeys; to Daisuke Doi, Bumpei Samata, Sadaharu Torikoshi, Takafumi Shimogawa, and Ryosuke Tsuchimochi for taking care of the animals; to Towa Pharmaceutical for Tacrolimus hydrate; to Peter Karagiannis for critical reading of the manuscript; and to all members of the Takahashi lab for fruitful discussions. This work was supported by a grant from the Network Program for Realization of Regenerative Medicine from the Japan Agency for Medical Research and Development (AMED) (18bm0204004h0006) (to J.T.), Japan Society for the Promotion of Science (JSPS) KAKENHI grant no. 17H04302 (to J.T.), JSPS KAKENHI grant nos. 16H06897 and 18K15046 (to H.S.), and Grant-in-Aid for JSPS Fellows (JSPS PD research fellowship grant no. 17J10294) (to H.S.).

Received: December 12, 2019
Revised: June 16, 2020
Accepted: June 18, 2020
Published: July 16, 2020

REFERENCES

Alcamo, E.A., Chirivella, L., Dautzenberg, M., Dobreva, G., Farinas, I., Grosschedl, R., and McConnell, S.K. (2008). Satb2 regulates callosal projection neuron identity in the developing cerebral cortex. Neuron *57*, 364–377.

Arlotta, P., Molyneaux, B.J., Chen, J., Inoue, J., Kominami, R., and Macklis, J.D. (2005). Neuronal subtype-specific genes that control corticospinal motor neuron development in vivo. Neuron *45*, 207–221.

Ballout, N., Frappe, I., Peron, S., Jaber, M., Zibara, K., and Gaillard, A. (2016). Development and maturation of embryonic cortical neurons grafted into the damaged adult motor cortex. Front. Neural Circuits *10*, 55.

Ballout, N., Rochelle, T., Brot, S., Bonnet, M.L., Francheteau, M., Prestoz, L., Zibara, K., and Gaillard, A. (2019). Characterization of inflammation in delayed cortical transplantation. Front. Mol. Neurosci. *12*, 160.

Britanova, O., de Juan Romero, C., Cheung, A., Kwan, K.Y., Schwark, M., Gyorgy, A., Vogel, T., Akopov, S., Mitkovski, M., Agoston, D., et al. (2008). Satb2 is a postmitotic determinant for upper-layer neuron specification in the neocortex. Neuron *57*, 378–392.

Chen, H.I., Wolf, J.A., Blue, R., Song, M.M., Moreno, J.D., Ming, G.L., and Song, H. (2019). Transplantation of human brain organoids: revisiting the science and ethics of brain chimeras. Cell Stem Cell *25*, 462–472.

Courtine, G., Bunge, M.B., Fawcett, J.W., Grossman, R.G., Kaas, J.H., Lemon, R., Maier, I., Martin, J., Nudo, R.J., Ramon-Cueto, A., et al. (2007). Can experiments in nonhuman primates expedite the translation of treatments for spinal cord injury in humans? Nat. Med. *13*, 561–566.

Cugola, F.R., Fernandes, I.R., Russo, F.B., Freitas, B.C., Dias, J.L., Guimaraes, K.P., Benazzato, C., Almeida, N., Pignatari, G.C., Romero, S., et al. (2016). The Brazilian Zika virus strain causes birth defects in experimental models. Nature *534*, 267–271.

Dang, J., Tiwari, S.K., Lichinchi, G., Qin, Y., Patil, V.S., Eroshkin, A.M., and Rana, T.M. (2016). Zika virus depletes neural progenitors in human cerebral organoids through activation of the innate immune receptor TLR3. Cell Stem Cell *19*, 258–265.

Daviaud, N., Friedel, R.H., and Zou, H. (2018). Vascularization and engraftment of transplanted human cerebral organoids in mouse cortex. eNeuro *5*, ENEURO.0219-18.2018.

Dwyer, N.D., Chen, B., Chou, S.J., Hippenmeyer, S., Nguyen, L., and Ghashghaei, H.T. (2016). Neural stem cells to cerebral cortex: emerging mechanisms regulating progenitor behavior and productivity. J. Neurosci. *36*, 11394–11401.

Eiraku, M., Watanabe, K., Matsuo-Takasaki, M., Kawada, M., Yonemura, S., Matsumura, M., Wataya, T., Nishiyama, A., Muguruma, K., and Sasai, Y. (2008). Self-organized formation of polarized cortical tissues from ESCs and its active manipulation by extrinsic signals. Cell Stem Cell *3*, 519–532.

Espuny-Camacho, I., Michelsen, K.A., Gall, D., Linaro, D., Hasche, A., Bonnefont, J., Bali, C., Orduz, D., Bilheu, A., Herpoel, A., et al. (2013). Pyramidal neurons derived from human pluripotent stem cells integrate efficiently into mouse brain circuits in vivo. Neuron *77*, 440–456.

Espuny-Camacho, I., Michelsen, K.A., Linaro, D., Bilheu, A., Acosta-Verdugo, S., Herpoel, A., Giugliano, M., Gaillard, A., and Vanderhaeghen, P. (2018). Human pluripotent stem-cell-derived cortical neurons integrate functionally into the lesioned adult murine visual cortex in an area-specific way. Cell Rep. *23*, 2732–2743.

Fame, R.M., MacDonald, J.L., and Macklis, J.D. (2011). Development, specification, and diversity of callosal projection neurons. Trends Neurosci. *34*, 41–50.

Gaillard, F., Domballe, L., and Gaillard, A. (2004). Fetal cortical allografts project massively through the adult cortex. Neuroscience *126*, 631–637.

Gaillard, A., Prestoz, L., Dumartin, B., Cantereau, A., Morel, F., Roger, M., and Jaber, M. (2007). Reestablishment of damaged adult motor pathways by grafted embryonic cortical neurons. Nat. Neurosci. *10*, 1294–1299.

Garcez, P.P., Loiola, E.C., Madeiro da Costa, R., Higa, L.M., Trindade, P., Delvecchio, R., Nascimento, J.M., Brindeiro, R., Tanuri, A., and Rehen, S.K. (2016). Zika virus impairs growth in human neurospheres and brain organoids. Science *352*, 816–818.

Gopinath, G., Mahapatra, A.K., Bharadwaj, J.C., Banerji, R., Sharma, D.N., and Tandon, P.N. (1989). Transplantation of fetal neocortex in rhesus monkey. J. Biosci. *14*, 255–260.

Grade, S., and Gotz, M. (2017). Neuronal replacement therapy: previous achievements and challenges ahead. NPJ Regen. Med. *2*, 29.

Greig, L.C., Woodworth, M.B., Galazo, M.J., Padmanabhan, H., and Macklis, J.D. (2013). Molecular logic of neocortical projection neuron specification, development and diversity. Nat. Rev. Neurosci. *14*, 755–769.

Heide, M., Huttner, W.B., and Mora-Bermudez, F. (2018). Brain organoids as models to study human neocortex development and evolution. Curr. Opin. Cell Biol. *55*, 8–16.

Hevner, R.F., Daza, R.A., Rubenstein, J.L., Stunnenberg, H., Olavarria, J.F., and Englund, C. (2003). Beyond laminar fate: toward a molecular classification of cortical projection/pyramidal neurons. Dev. Neurosci. *25*, 139–151.

Kadoshima, T., Sakaguchi, H., Nakano, T., Soen, M., Ando, S., Eiraku, M., and Sasai, Y. (2013). Self-organization of axial polarity, inside-out layer pattern, and species-specific progenitor dynamics in human ES cell-derived neocortex. Proc. Natl. Acad. Sci. U S A *110*, 20284–20289.

Kwan, K.Y., Sestan, N., and Anton, E.S. (2012). Transcriptional co-regulation of neuronal migration and laminar identity in the neocortex. Development *139*, 1535–1546.

Lancaster, M.A., Renner, M., Martin, C.A., Wenzel, D., Bicknell, L.S., Hurles, M.E., Homfray, T., Penninger, J.M., Jackson, A.P., and Knoblich, J.A. (2013). Cerebral organoids model human brain development and microcephaly. Nature *501*, 373–379.

Lemon, R.N. (2008). Descending pathways in motor control. Annu. Rev. Neurosci. *31*, 195–218.

Leyva-Diaz, E., and Lopez-Bendito, G. (2013). In and out from the cortex: development of major forebrain connections. Neuroscience *254*, 26–44.

Liauw, J., Hoang, S., Choi, M., Eroglu, C., Choi, M., Sun, G.H., Percy, M., Wildman-Tobriner, B., Bliss, T., Guzman, R.G., et al. (2008). Thrombospondins 1 and 2 are necessary for synaptic

plasticity and functional recovery after stroke. J. Cereb. Blood Flow Metab. *28*, 1722–1732.

Lindvall, O., and Kokaia, Z. (2011). Stem cell research in stroke: how far from the clinic? Stroke *42*, 2369–2375.

Mansour, A.A., Goncalves, J.T., Bloyd, C.W., Li, H., Fernandes, S., Quang, D., Johnston, S., Parylak, S.L., Jin, X., and Gage, F.H. (2018). An in vivo model of functional and vascularized human brain organoids. Nat. Biotechnol. *36*, 432–441.

Molyneaux, B.J., Arlotta, P., Menezes, J.R., and Macklis, J.D. (2007). Neuronal subtype specification in the cerebral cortex. Nat. Rev. Neurosci. *8*, 427–437.

Palma-Tortosa, S., Tornero, D., Gronning Hansen, M., Monni, E., Hajy, M., Kartsivadze, S., Aktay, S., Tsupykov, O., Parmar, M., Deisseroth, K., et al. (2020). Activity in grafted human iPS cell-derived cortical neurons integrated in stroke-injured rat brain regulates motor behavior. Proc. Natl. Acad. Sci. U S A *117*, 9094–9100.

Peron, S., Droguerre, M., Debarbieux, F., Ballout, N., Benoit-Marand, M., Francheteau, M., Brot, S., Rougon, G., Jaber, M., and Gaillard, A. (2017). A delay between motor cortex lesions and neuronal transplantation enhances graft integration and improves repair and recovery. J. Neurosci. *37*, 1820–1834.

Qian, X., Nguyen, H.N., Song, M.M., Hadiono, C., Ogden, S.C., Hammack, C., Yao, B., Hamersky, G.R., Jacob, F., Zhong, C., et al. (2016). Brain-region-specific organoids using mini-bioreactors for modeling ZIKV exposure. Cell *165*, 1238–1254.

Quadrato, G., and Arlotta, P. (2017). Present and future of modeling human brain development in 3D organoids. Curr. Opin. Cell Biol. *49*, 47–52.

Sakaguchi, H., Ozaki, Y., Ashida, T., Matsubara, T., Oishi, N., Kihara, S., and Takahashi, J. (2019). Self-organized synchronous calcium transients in a cultured human neural network derived from cerebral organoids. Stem Cell Reports *13*, 458–473.

Samata, B., Takaichi, R., Ishii, Y., Fukushima, K., Nakagawa, H., Ono, Y., and Takahashi, J. (2020). L1CAM is a marker for enriching corticospinal motor neurons in the developing brain. Front. Cell. Neurosci. *14*, 31.

Sano, N., Shimogawa, T., Sakaguchi, H., Ioroi, Y., Miyawaki, Y., Morizane, A., Miyamoto, S., and Takahashi, J. (2017). Enhanced axonal extension of subcortical projection neurons isolated from murine embryonic cortex using Neuropilin-1. Front. Cell. Neurosci. *11*, 123.

Sawai, T., Sakaguchi, H., Thomas, E., Takahashi, J., and Fujita, M. (2019). The ethics of cerebral organoid research: being conscious of consciousness. Stem Cell Reports *13*, 440–447.

Skold, M.K., von Gertten, C., Sandberg-Nordqvist, A.C., Mathiesen, T., and Holmin, S. (2005). VEGF and VEGF receptor expression after experimental brain contusion in rat. J. Neurotrauma *22*, 353–367.

Suzuki, I.K., and Vanderhaeghen, P. (2015). Is this a brain which I see before me? Modeling human neural development with pluripotent stem cells. Development *142*, 3138–3150.

Toma, K., and Hanashima, C. (2015). Switching modes in corticogenesis: mechanisms of neuronal subtype transitions and integration in the cerebral cortex. Front. Neurosci. *9*, 274.

Tornero, D., Wattananit, S., Gronning Madsen, M., Koch, P., Wood, J., Tatarishvili, J., Mine, Y., Ge, R., Monni, E., Devaraju, K., et al. (2013). Human induced pluripotent stem cell-derived cortical neurons integrate in stroke-injured cortex and improve functional recovery. Brain *136*, 3561–3577.

Tornero, D., Tsupykov, O., Granmo, M., Rodriguez, C., Gronning-Hansen, M., Thelin, J., Smozhanik, E., Laterza, C., Wattananit, S., Ge, R., et al. (2017). Synaptic inputs from stroke-injured brain to grafted human stem cell-derived neurons activated by sensory stimuli. Brain *140*, 692–706.

Watanabe, M., Buth, J.E., Vishlaghi, N., de la Torre-Ubieta, L., Taxidis, J., Khakh, B.S., Coppola, G., Pearson, C.A., Yamauchi, K., Gong, D., et al. (2017). Self-organized cerebral organoids with human-specific features predict effective drugs to combat Zika virus infection. Cell Rep. *21*, 517–532.

Wuttke, T.V., Markopoulos, F., Padmanabhan, H., Wheeler, A.P., Murthy, V.N., and Macklis, J.D. (2018). Developmentally primed cortical neurons maintain fidelity of differentiation and establish appropriate functional connectivity after transplantation. Nat. Neurosci. *21*, 517–529.

Stem Cell Reports, Volume *15*

Supplemental Information

Axonal Extensions along Corticospinal Tracts from Transplanted Human Cerebral Organoids

Takahiro Kitahara, Hideya Sakaguchi, Asuka Morizane, Tetsuhiro Kikuchi, Susumu Miyamoto, and Jun Takahashi

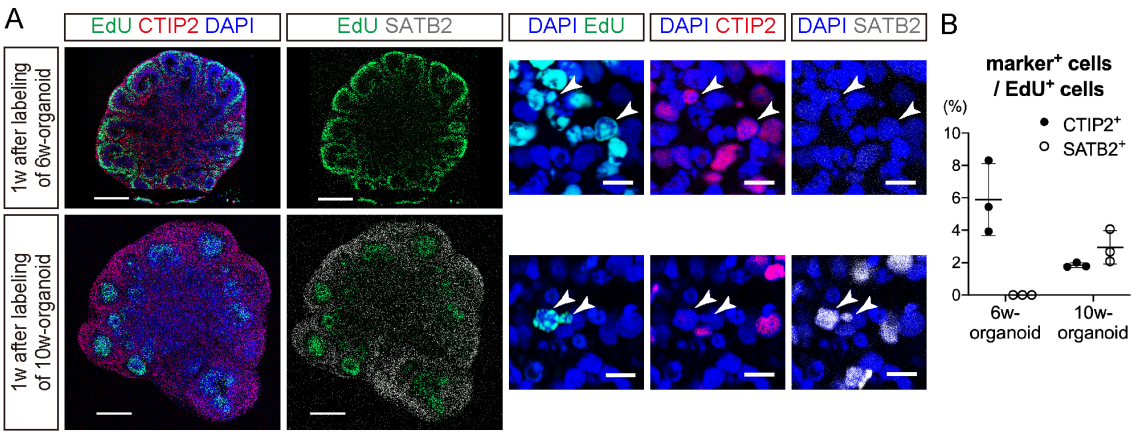

Figure S1

Marker expression by newly generated cells in 6w- and 10w-organoids. Related to Figure 1

(A) Immunohistochemistry for EdU, CTIP2, and SATB2 one week (1w) after EdU labeling dividing cells in 6w- and 10w-organoids. Scale bars, 500 μm (two leftmost columns) and 10 μm (other columns).

(B) Percentages of $CTIP2^+$ cells and $SATB2^+$ cells in EdU^+ cells 1w after EdU labeling 6w- and 10w-organoids. $EdU^+/SATB2^+$ cells were absent in 6w-organoids but observed in 10w-organoids. n = 3 for both organoids (n: number of aggregates). Results are presented as the mean ± standard deviation.

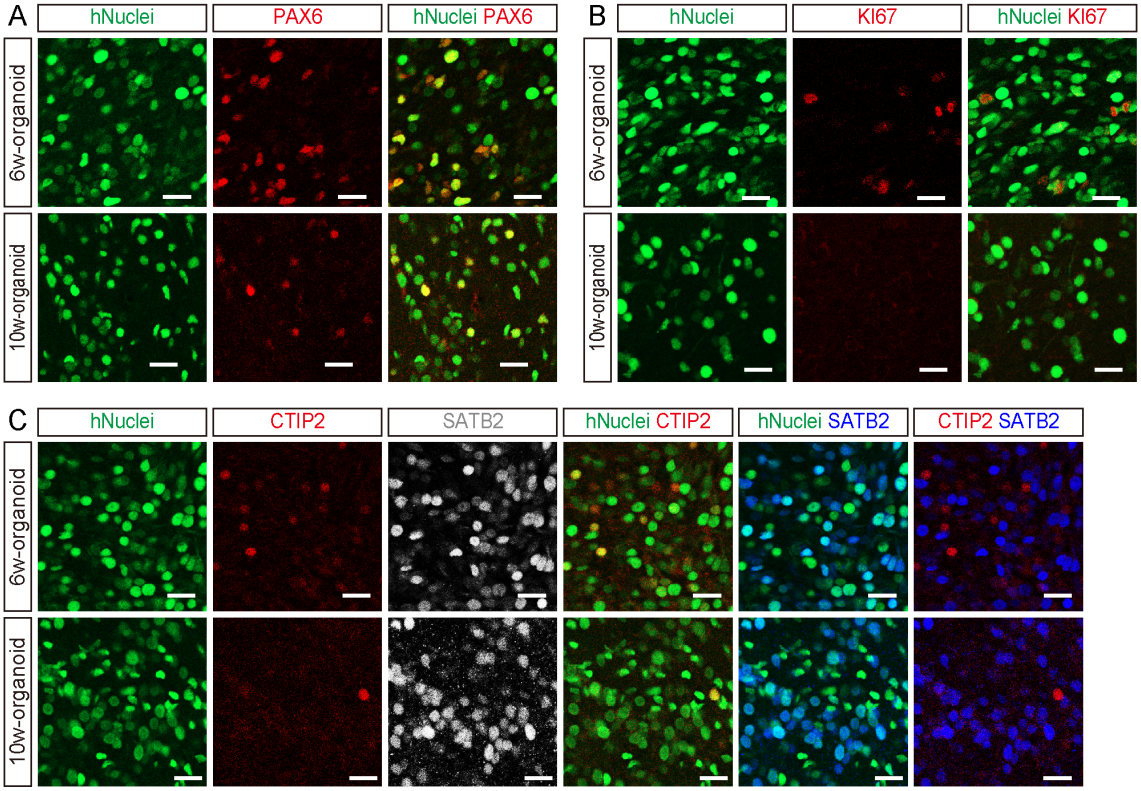

Figure S2

Marker expression for proliferative cells and projection neurons in engrafted cerebral organoids. Related to Figure 4

Immunohistochemistry for PAX6 (A), KI67 (B), CTIP2, and SATB2 (C) co-expressed with hNuclei^{+} cells in engrafted 6w- and 10w-organoids. Scale bars, 20 μm.

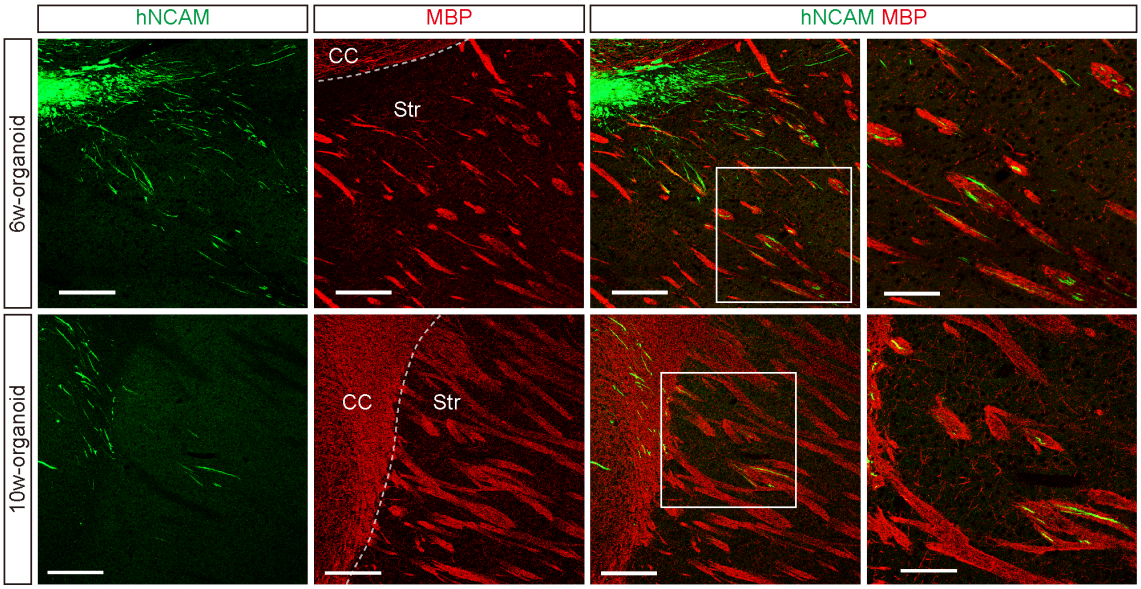

Figure S3

Graft-derived fibers were elongated along myelinated bundles in the striatum. Related to Figure 5

Immunohistochemistry for hNCAM and MBP in the host striatum at 12 wpt. The rightmost column shows higher magnification images of the boxed areas. Scale bars, 200 μm (left three columns) and 100 μm (rightmost column).

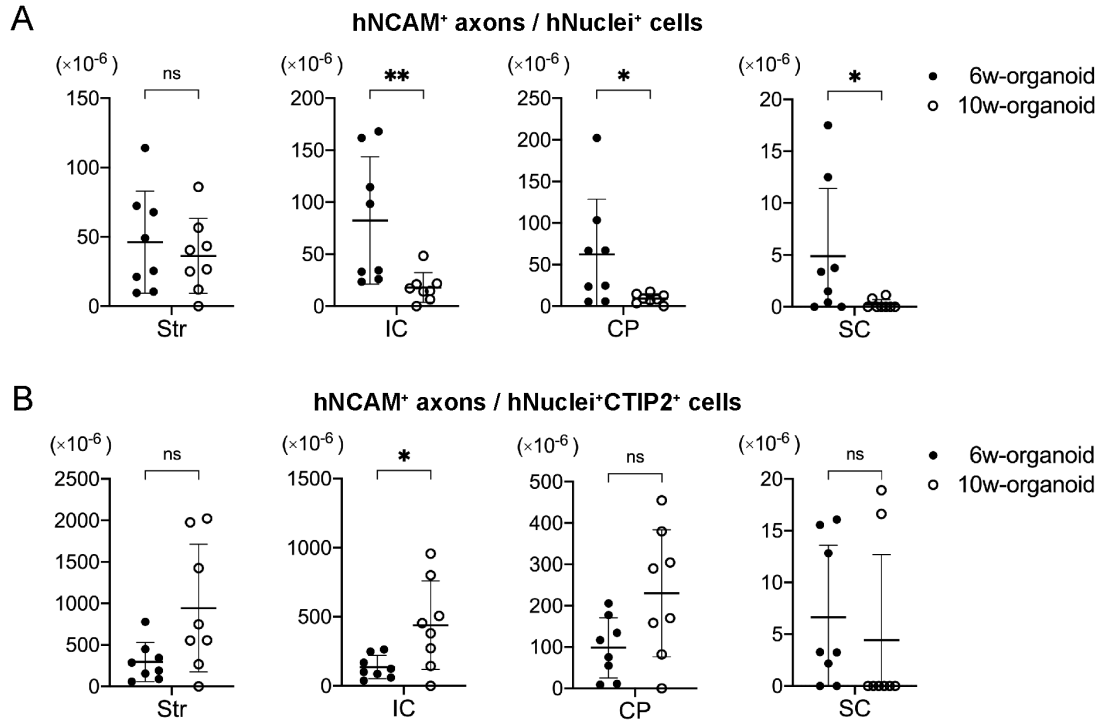

Figure S4

Number of graft-derived axons per cell. Related to Figure 5

(A) Number of axons per engrafted hNuclei$^+$ cell. n = 8 for 6w- and 10w-organoids (n: number of mice). * $p < 0.05$, ** $p < 0.01$, ns: not significant, Mann-Whitney test. Results are presented as the mean ± standard deviation.

(B) Number of axons per engrafted hNuclei$^+$/CTIP2$^+$ cell. n = 8 for both organoids (n: number of mice). * $p < 0.05$, ns: not significant, Mann-Whitney test. Results are presented as the mean ± standard deviation.

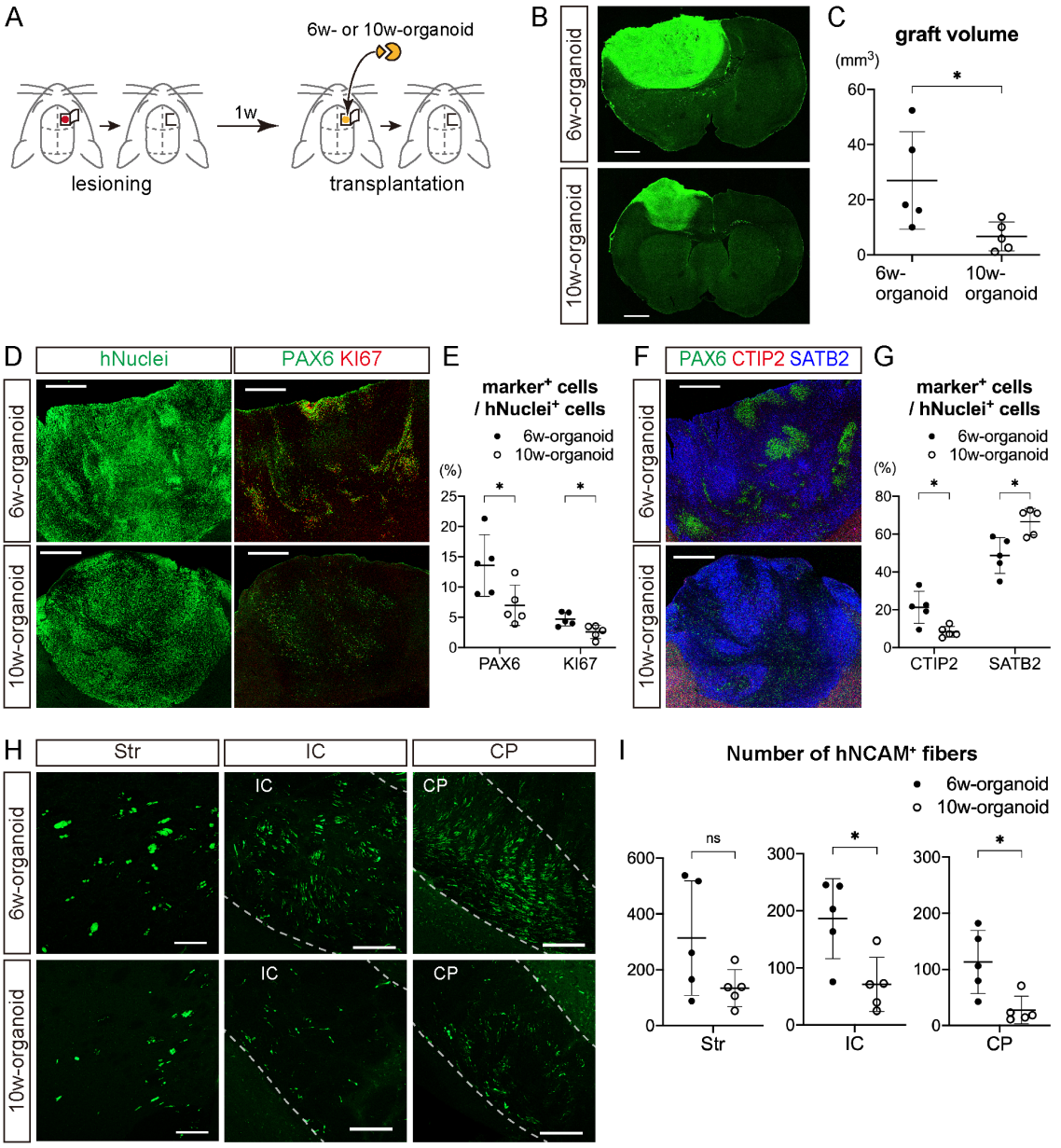

Figure S5

Transplantation of 6w- or 10w-organoids into 6-week-old mice with one-week delay after lesioning. Related to Figure 2, 4, and 5

(A) Schematic of the procedure for the transplantation of 6w- or 10w-organoids into the right frontal cortex of 6-week-old mice with one-week delay after making the cavity. n = 5 for both 6w- and 10w-organoids (n: number of mice).

(B) Immunohistochemistry (IHC) for hNCAM in coronal sections of mouse brains at 12 wpt. Upper: Bregma + 0.90 mm, lower: Bregma + 1.08 mm. Scale bars, 1 mm.

(C) The graft volume at 12 wpt. n = 5 for both organoids (n: number of mice). * $p < 0.05$, Mann-Whitney test. Results are presented as the mean ± standard deviation.

(D) IHC for hNuclei, PAX6, and KI67 in the engrafted tissues at 12 wpt. Scale bars, 500 μm.

(E) Percentages of $PAX6^+$ cells and $KI67^+$ cells in $hNuclei^+$ cells in the engrafted tissues at 12 wpt. n = 5 for both organoids (n: number of mice). * $p < 0.05$, Mann-Whitney test. Results are presented as the mean ± standard deviation.

(F) IHC for CTIP2, SATB2, and PAX6 in the engrafted tissues at 12 wpt. Scale bars, 500 μm.

(G) Percentages of $CTIP2^+$ cells and $SATB2^+$ cells in $hNuclei^+$ cells at 12 wpt. n = 5 for both organoids (n: number of mice). * $p < 0.05$, Mann-Whitney test. Results are presented as the mean ± standard deviation.

(H) IHC for hNCAM in coronal sections of mouse brain shows graft-derived axonal extensions in the striatum (Str), internal capsule (IC), and cerebral peduncle (CP) of the host at 12 wpt. Scale bars, 100 μm.

(I) Number of $hNCAM^+$ fibers in the Str, IC, and CP of the host at 12 wpt. n = 5 for both organoids (n: number of mice). ns: not significant, * $p < 0.05$, Mann-Whitney test. Results are presented as the mean ± standard deviation.

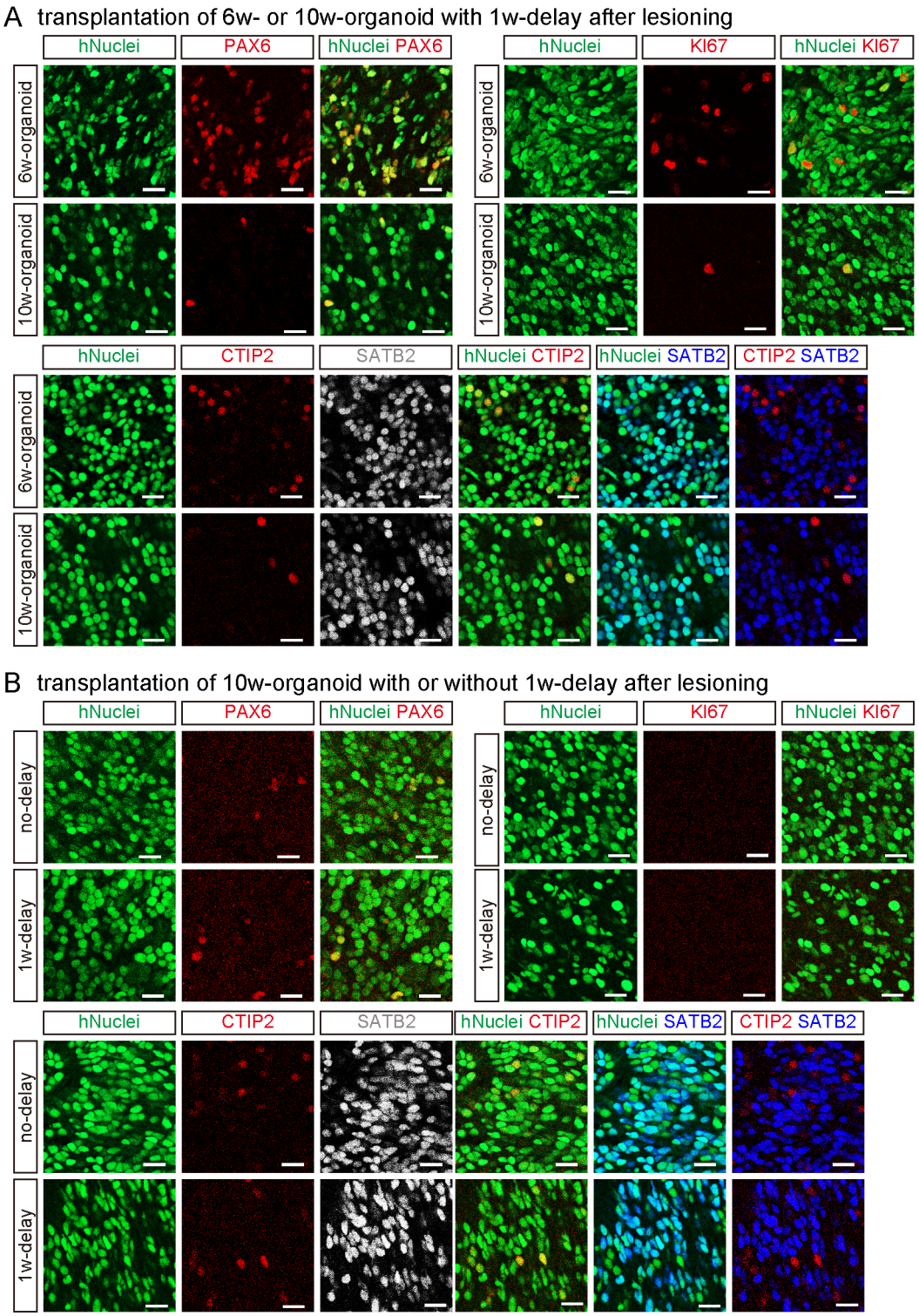

Figure S6

6w-organoids after transplantation with one-week delay (1w-delay) contained more proliferative cells, and 10w-organoids after transplantation with and without 1w-delay contained few proliferative cells. Related to Figure 5 and 6

Immunohistochemistry for PAX6, KI67, CTIP2, and SATB2 co-expressed with hNuclei^{+} cells after the transplantation of 6w- or 10w-organoids with 1w-delay (A) and after transplantation of 10w-organoids with or without 1w-delay (B). Scale bars, 20 μm.

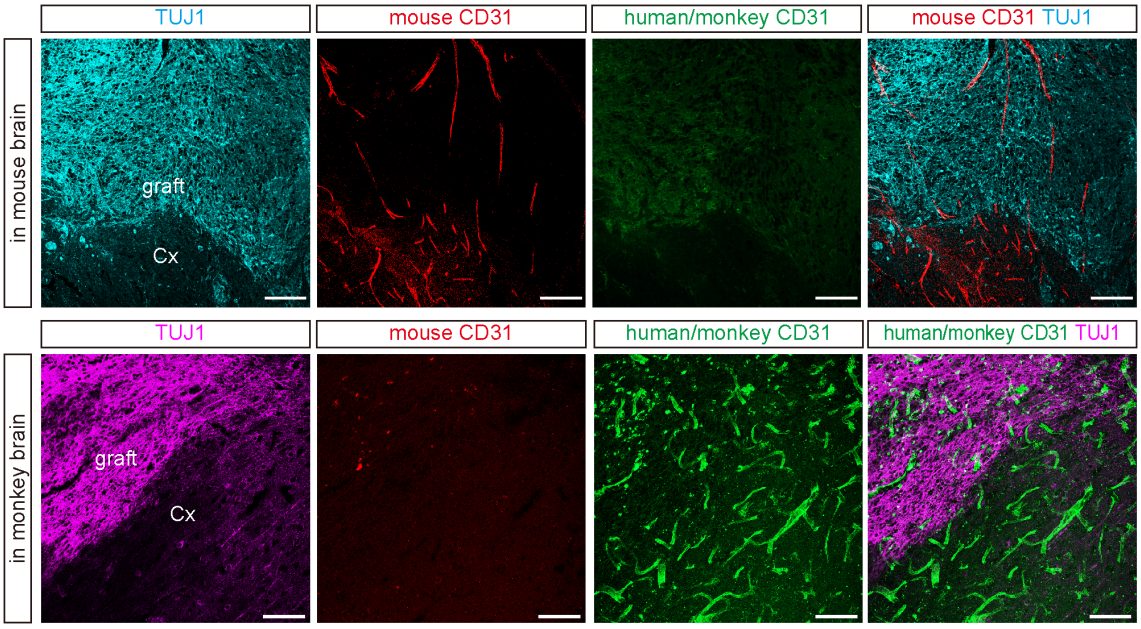

Figure S7

Reactivities with mouse- and human/monkey-specific CD31 antibodies was consistent between blood vessels in the engrafted organoids and blood vessels in the host brain.

Immunohistochemistry for TUJ1, mouse-specific CD31, and human/monkey-specific CD31 in cerebral organoids engrafted in mouse brain (upper row) and monkey brain (lower row). Cx: cerebral cortex. Scale bars, 100 μm.

Supplemental Experimental Procedures

Maintenance Culture of Human Embryonic Stem Cells (hESCs)

All experiments using hESCs were approved by the Ethics Committee of Kyoto University Graduate School and Faculty of Medicine. hESCs were used in accordance with 'The Guidelines for Derivation and Utilization of Human Embryonic Stem Cells' of the Ministry of Education, Culture, Sports, Science and Technology of Japan. hESCs were maintained and cultured as previously described (Sakaguchi et al., 2019). In brief, hESCs (KhES-1) were maintained on a feeder layer of mouse embryonic fibroblasts (Oriental Yeast) inactivated by 10 μg/ml mitomycin C (Wako) treatment in DMEM/F12 (Sigma-Aldrich) supplemented with 20% (vol/vol) Knockout Serum Replacement (KSR; Gibco), 2 mM L-glutamine (Gibco), 0.1 mM non-essential amino acids (NEAA; Gibco), 5 ng/ml recombinant human basic fibroblast growth factor (Wako), 0.1 mM 2-mercaptoethanol (2-ME; Wako), 100 U/ml penicillin, and 100 μg/ml streptomycin (Gibco) under 2% CO_2. Medium change was performed once every day. For passaging, hESC colonies were detached and recovered en bloc from the feeder layer by treating them with 0.25% (wt/vol) trypsin (Gibco) and 1 mg/ml collagenase IV (Gibco) in phosphate buffered saline (PBS) containing 20% (vol/vol) KSR and 1 mM $CaCl_2$ (Wako) at 37°C for 8 min. The detached hESC clumps were broken into smaller pieces by gentle pipetting. The passages were performed at a 1:4–1:6 split ratio every 3–4 days.

Differentiation Culture of hESCs

The differentiation culture of hESCs was performed using the SFEBq (serum-free floating culture of embryoid body-like aggregates with quick reaggregation) method as previously described (Sakaguchi et al., 2019). In brief, hESCs were dissociated to single cells in TrypLE Express (Gibco) containing 1.25 U/ml DNase I (Takara Bio) and 10 μM Y-27632 (Wako), and quickly reaggregated using low-cell-adhesion-coated V-bottomed 96-well plates (PrimeSurface MS-9096V; Sumitomo Bakelite) in differentiation medium (9,000 cells per well, 100 μl) under 5% CO_2. The differentiation medium was Glasgow's MEM (Gibco) supplemented with 20% (vol/vol) KSR, 0.1 mM NEAA, 1 mM sodium pyruvate (Sigma-Aldrich), 0.1 mM 2-ME, 100 U/ml penicillin, and 100 μg/ml streptomycin. Defining the day on which the SFEBq culture was started as day 0, 5 μM SB431542 (transforming growth factor β inhibitor; TOCRIS) and 3 μM IWR1e (Wnt inhibitor; Calbiochem) were added to the culture from day 0 to day 18. 50 μM Y-27632

was added from day 0 to day 3. Half the medium was changed once every 3 days from day 3 to day 15. At day 18, the floating aggregates were transferred to 10-mm non-adhesive dishes (EZSPHERE; Iwaki) and further cultured in suspension using DMEM/F-12 GlutaMAX (Gibco) supplemented with 1% (vol/vol) N-2 Supplement (Gibco), 1% (vol/vol) Chemically Defined Lipid Concentrate (CDLC; Gibco), 0.25 μg/ml Amphotericin B (Gibco), 100 U/ml penicillin, and 100 μg/ml streptomycin under 40% O_2/5% CO_2 conditions. The floating aggregates were cut into halves or thirds with micro scissors (Bio Research Center, #16324319) under a stereo microscope at day 35, and the aggregates were transferred to gas-permeable dishes (Lumox dish; Sarastedt) at day 50. All medium was changed once every 3 days after day 18. When 5-ethynyl-2'-deoxyuridine (EdU) labeling of 6w- or 10w-organoids was performed, 10 μM EdU (Sigma-Aldrich) was added to the medium for 24 h.

Magnetic Resonance Imaging (MRI)

The monkeys were subjected to MRI study before and immediately after transplantation, and once every month thereafter. Animals were anesthetized with ketamine (10 mg/kg) and xylazine (1 mg/kg), and T1- and T2-weighted images were obtained using a 3-tesla MRI scanner (MAGNETOM Verio, Siemens Healthcare).

Brain Tissue Collection and Sample Fixation

Mice and monkeys were euthanized at 12 weeks post-transplantation (wpt). For mice, pentobarbital (200 mg/kg, intraperitoneally) was administrated, and transcardial perfusion was performed with PBS followed by 4% PFA. Brains were dissected and post-fixed in 4% paraformaldehyde (PFA) overnight at 4°C. Brains were cryoprotected in 15% sucrose in PBS (4°C, overnight) followed by 30% sucrose in PBS (4°C, two overnight). For monkeys, transcardial perfusion was performed with PBS followed by 4% PFA under deep anesthesia with pentobarbital (100 mg/kg, intravenously). Brains were post-fixed in 4% PFA (4°C, 24 h) and then cryoprotected in 10% sucrose in PBS at 4°C for 1–2 days, in 20% sucrose in PBS at 4°C for 2–3 days, and finally in 30% sucrose in PBS at 4°C for 3–4 days.

In vitro samples of cerebral organoids were fixed in 4% PFA at 4°C for 15–30 min and then cryoprotected in 15% sucrose in PBS (4°C, overnight) followed by 30% sucrose in PBS (4°C, overnight).

Immunofluorescence Staining and Histological Processing

The sample sectioning was performed with a cryostat (CM 3050S; Leica). *In vitro* samples of cerebral organoids were sliced at 12 μm thickness. Mouse brains were sliced coronally or sagittally at 30 μm thickness. Monkey brains were sliced coronally at 40 μm thickness.

In vitro samples were attached to coated glass slides (MAS-01; Matsunami Glass) before immunohistochemical staining. *In vivo* samples of animal brains were stained using the free-floating method before attachment to coated glass slides (APS-01; Matsunami Glass).

Samples were permeabilized with 0.3% Triton X-100 (Sigma-Aldrich) in PBS (room temperature, 45 min), blocked with 2% Skim Milk (Difco) in PBS (room temperature, 30–60 min), and incubated with primary antibodies (4°C, overnight) followed by incubation with secondary antibodies conjugated with Alexa 488, 594, and 647 (room temperature, 2 h). The primary antibodies were used at the following dilutions: FOXG1 (rabbit, 1:1,000, Takara Bio, M227), MAP2 (mouse, 1:200, Sigma, M4403), PAX6 (mouse, 1:500, BD, 561462), PAX6 (rabbit, 1:500, BioLegend, 901301), CTIP2 (rat, 1:1,000, abcam, ab18465), SATB2 (mouse, 1:200, abcam, ab515020), SATB2 (rabbit, 1:500, abcam, ab34735), KI67 (rabbit, 1:1,000, Novocastra, NCL-ki67p), hNCAM (mouse, 1:500, Santa Cruz, sc-106), hNuclei (mouse, 1:1,000, Millipore, MAB1281), STEM121 (mouse, 1:500, Cellartis, Y40410), TUJ1 (rabbit, 1:1,000, Covance, PRB-435P), mouse CD31 (rat, 1:250, BD, 553370), human/monkey CD31 (mouse, 1:200, abcam, ab199012), and MBP (rat, 1:1,000, Millipore, MAB386). Counter nuclear staining was performed with 4′,6-diamidino-2-phenylindole (DAPI). EdU was detected with the Click-iT EdU Alexa Fluor 488 Imaging Kit (Invitrogen).

Quantitative Analysis

The thickness of layers in the cerebral organoids was measured with Fiji software (Schindelin et al., 2012). 10 and 13 aggregates were analyzed for 6w-organoid and for 10w-organoids, and 4.7 ± 1.5 layers and 5.7 ± 1.0 layers were measured in each aggregate, respectively.

Quantification of the graft volume and the host brain volume was performed by hNCAM immunostaining every six slices after sectioning at 30 μm thickness. The graft

area and the host brain area in each slice were measured with Fiji software. The host brain area was measured after excluding the olfactory bulb, cerebellum, and the brain stem. The volumes were calculated with the following formula: V (mm^3) = (S1 + S2 + ... + Sn) × 0.18, where S is the area (mm^2) of the graft or the host brain in each slice, and n is the number of slices.

Cell counting for marker expression analyses was performed with CellPathfinder software (Yokogawa), except for the analysis of co-expression of EdU and markers *in vitro*, which was performed by manual counting. *In vitro*, 10 and 13 aggregates were analyzed for 6w-organoids and 10w-organoids, and 76492 ± 22216 cells and 131300 ± 26162 cells were counted in each aggregate, respectively. Regarding the co-expression of EdU and markers, three aggregates were analyzed each for 6w-organoids and for 10w-organoids, and 300 ± 6 EdU^+ cells and 270 ± 87 EdU^+ cells were counted in each aggregate, respectively. In mice with four transplant sites, the average percentage in all the survived grafts in each mouse was used for the analysis. 15204 ± 9667 cells and 4600 ± 4362 cells were counted in each graft for 6w-organoids and for 10w-organoids, respectively. In mice with one transplant site, the average percentage in three slices in each mouse was used for the analysis. In the transplantation of 6w- or 10w-organoids into 6-week-old mice, 46740 ± 20202 cells and 15280 ± 11840 cells were counted in each slice, respectively. In the transplantation of 10w-organoids into 6-week-old mice with or without one-week delay, 5153 ± 2584 cells and 27224 ± 12442 cells were counted in each slice for the no-delay group and for the 1w-delay group, respectively.

The number of cells contained in the organoids after cutting *in vitro* was counted manually after dissociating the pieces of organoids with the papain-containing Enzyme Solution of Neural Tissue Dissociation Kit (Sumitomo Bakelite, MB-X9901). Six organoids were analyzed each for 6w-organoids and for 10w-organoids. The estimated number of graft-derived cells in the engrafted tissues was calculated with hNuclei immunostaining after sectioning at 30 μm thickness and with the following formula: $N = V \times n / (S \times 0.03)$, where V ($mm^3$) is the graft volume, n is the sum of numbers of $hNuclei^+$ cells in the analyzed sections, and S (mm^2) is the sum of the graft areas in the analyzed sections. Four slices in each mouse were used for the analysis. 16857 ± 10052 cells and 5080 ± 4101 cells were counted in each slice for 6w-organoids and for 10w-organoids, respectively. The estimated number of graft-derived $CTIP2^+$ cells in the graft was calculated with the estimated number of $hNuclei^+$ cells and the percentage of $CTIP2^+$ cells

in the graft.

Fiber counting was performed with Fiji software after binarizing the images of each target area with the software. Three slices were analyzed for each part of all mice. The region of interest in each slice was decided based on the anatomical structures observed in the hNCAM immunostaining. In mice with four transplant sites, average numbers in both hemispheres in each mouse were used for the analyses.

The quantification of the $CD31^+$ area was performed with Fiji software after excluding areas with unspecific staining and after binarizing the images with the software. In mice with four transplant sites, the average percentage in all the survived grafts in each mouse was used for the analysis. In mice with one transplant site, the average percentage in three slices in each mouse was used for the analysis.

Supplemental References

Sakaguchi, H., Ozaki, Y., Ashida, T., Matsubara, T., Oishi, N., Kihara, S., and Takahashi, J. (2019). Self-Organized Synchronous Calcium Transients in a Cultured Human Neural Network Derived from Cerebral Organoids. Stem Cell Reports *13*, 458-473.

Schindelin, J., Arganda-Carreras, I., Frise, E., Kaynig, V., Longair, M., Pietzsch, T., Preibisch, S., Rueden, C., Saalfeld, S., Schmid, B.*, et al.* (2012). Fiji: an open-source platform for biological-image analysis. Nat Methods *9*, 676-682.